UCRL 3733

UNIVERSITY OF CALIFORNIA

Radiation Laboratory

COINCIDENCE NUCLEAR SPECTROMETRY WITH APPLICATIONS TO EUROPIUM-154 AND EUROPIUM-155

BERKELEY, CALIFORNIA

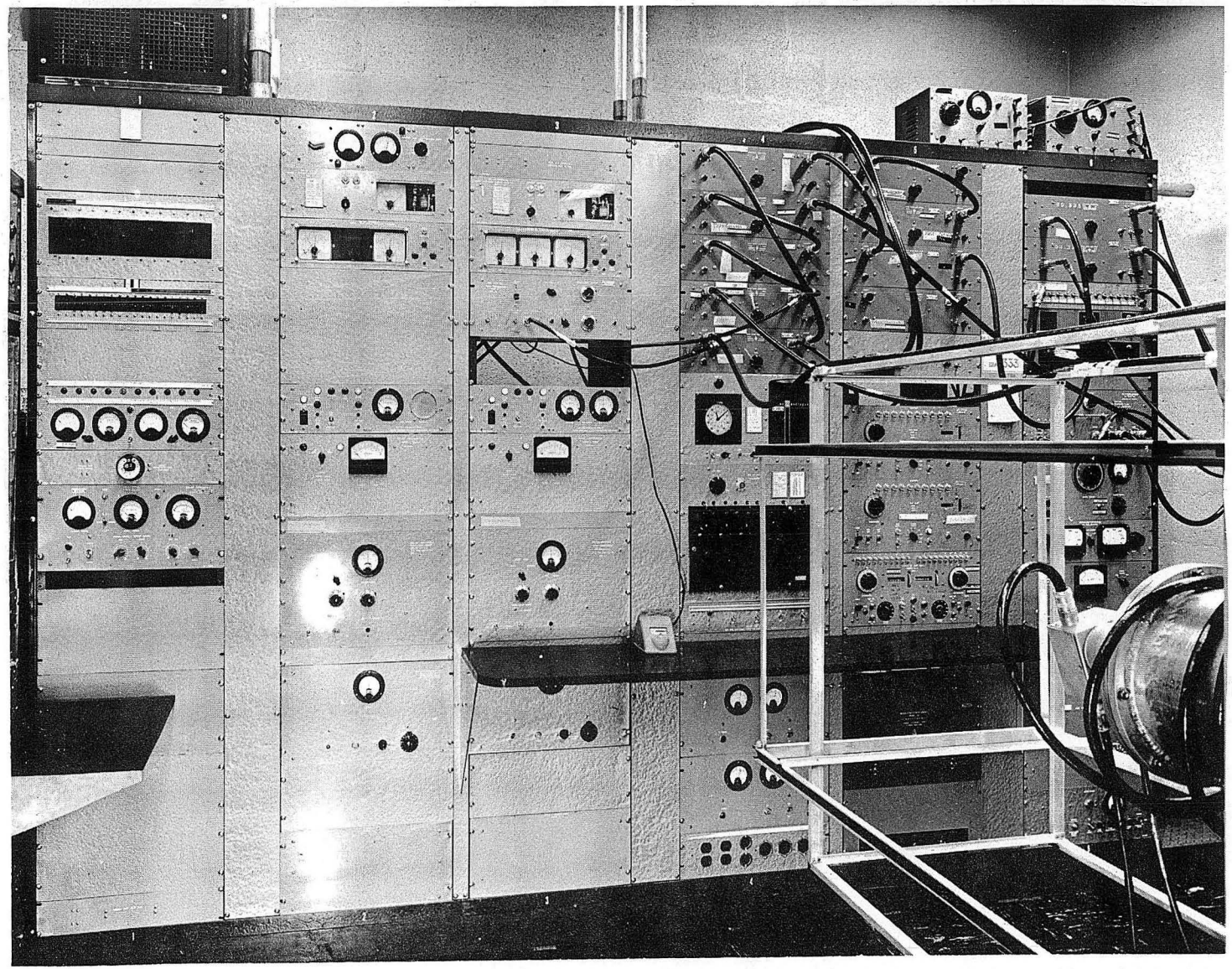

ZN-1696

Fig. 2. Control and counting panel for the electron-electron coincidence spectrometer.

UCRL-3733
Chemistry-General

UNIVERSITY OF CALIFORNIA

Radiation Laboratory
Berkeley, California

Contract No. W-7405-eng-48

COINCIDENCE NUCLEAR SPECTROMETRY WITH APPLICATIONS TO EUROPIUM-154 AND EUROPIUM-155

Jose O. Juliano
(Thesis)

April 1957

Printed for the U. S. Atomic Energy Commission

COINCIDENCE NUCLEAR SPECTROMETRY WITH APPLICATIONS TO EUROPIUM-154 AND EUROPIUM-155

Contents

Abstract 4

I. AN IRON-FREE BETA-RAY SPECTROMETER FOR ELECTRON-ELECTRON COINCIDENCES 5

A. Introduction 5

B. Description of the spectrometer 9

1. Spectrometer and vacuum tank 9

2. Vacuum system 11

3. Baffle system 12

4. Magnetic coils 14

a. Main coils 14

b. Trimmer coils 16

5. Cooling system 17

6. Magnet power supply 19

7. Earth's field compensating coils 22

8. Electron detectors 23

9. Coincidence circuit 24

10. Sources 26

C. Testing and operation characteristics of the spectrometer 27

1. Ring focusing baffle 27

2. Transmission of the spectrometer 28

3. Effect of trimmer coils on the operation of the spectrometer 31

4. Calibration of the spectrometer 31

5. Time-to-height converter calibration 37

6. Electron-electron coincidences in Bi^{207} 39

7. Electron-electron coincidences in Hg^{203} 41

II. DECAY OF EUROPIUM-154 43

A. Introduction 43

B. Experimental 45

1. Conversion electron results 45

2. Gamma-ray spectrum and gamma-gamma coincidence 47
3. Electron-electron coincidences 53
4. Decay scheme 56
C. Discussions 63
III. DECAY OF EUROPIUM-155 66
A. Introduction 66
B. Experimental 67
1. Conversion electron measurements 67
2. Assignment of multipolarities in the transitions 67
3. Decay scheme 75
IV. DECAY OF THORIUM-231 80
A. Introduction 80
B. Experimental 80
1. Beta components of Th^{231} 80
2. Relative intensities of the conversion lines and their multipolarities 81
Acknowledgments 98
List of Tables 99
List of Figures 100
References 102

COINCIDENCE NUCLEAR SPECTROMETRY WITH APPLICATIONS TO EUROPIUM-154 AND EUROPIUM-155

Jose O. Juliano

Radiation Laboratory and Department of Chemistry
University of California, Berkeley, California

April, 1957

ABSTRACT

An iron-free beta-ray spectrometer for electron-electron or electron-gamma coincidences using a time-to-height-converter as a coincidence unit was constructed, tested with Bi^{207} and Hg^{203}, and used in the study of the decay of Eu^{154}.

From the conversion-electron and gamma-ray data a decay scheme is proposed for Eu^{154} and Eu^{155}. Spins, parities, and quantum numbers of Nilsson's wave functions were assigned to the excited states whenever possible from the transition multipolarities.

The relative intensities of the stronger conversion-electron lines of Th^{231} were determined with a thin-window magnetic spectrometer, and multipolarities were assigned based on the K-conversion coefficients of Sliv and the L and M subshell conversion coefficients of Rose et al.

COINCIDENCE NUCLEAR SPECTROMETRY WITH APPLICATIONS TO EUROPIUM-154 AND EUROPIUM-155

Jose O. Juliano

Radiation Laboratory and Department of Chemistry
University of California, Berkeley, California

I. AN IRON-FREE BETA-RAY SPECTROMETER FOR ELECTRON-ELECTRON COINCIDENCES

A. INTRODUCTION

As the knowledge of nuclear energy levels advances each year, the need for coincidence spectrometers becomes more and more apparent. The state has been reached where mere numerology of the transitions involved, as determined from conversion-electron energies and gamma-ray spectra, is often not of much help in the final analysis of the problem. This is especially true when extremely complex spectra are encountered, a common occurrence in the heavy-element region. In cases in which moderate resolution is sufficient, measurement of gamma-gamma coincidences has been very useful and is still the most reliable method. However, for more complicated nuclides a higher-resolution instrument is needed to enable us to select with confidence only the transitions whose energies are being studied. The obvious resort is to use the conversion lines associated with the transitions and to find out which of these are in coincidence. This method has been used to advantage and electron-gamma coincidence spectrometers have been built. However, in extreme cases (i.e., with very complicated gamma spectra where so many transitions occur in the same energy range that the gamma spectrum appears like a continuous distribution) there is no other choice but to use an electron-electron coincidence spectrometer. This is in spite of the lower transmission inherent in electron spectrometers as compared with gamma analyzers, and the fact that the number of events may be further reduced by the conversion coefficients of the transitions being studied, which are usually small for high-energy transitions. With these two problems in mind, it is expected that the use of electron-electron coincidence spectrometers would also have its own limitations. However,

it would be a powerful tool when used in conjunction with the conventional instruments of analysis.

Numerous types of spectrometers have been built and described in the literature,[1-6] both for straight electron spectroscopy and for coincidence spectroscopy using electron-electron or electron-gamma techniques; hence no review is given in this report. Each type of spectrometer has its own merits as to resolution, transmission, data gathering, and initial cost, yet no single type can be said to be superior to the rest. The characteristics of various spectrometers have already been discussed in detail.[3]

It was decided to build two thin-lens iron-free beta-ray spectrometers joined back-to-back at the source ends for electron-electron coincidence spectroscopy. The finished instrument is shown in Figs. 1 and 2. In this fashion two different energy-conversion lines or beta particles can be focused and independently counted on either side of the instrument and the pulses fed into a regular coincidence circuit. For increased flexibility, the instrument was also designed to be easily converted into a gamma-electron coincidence spectrometer by placing a regular NaI (Tl) crystal at the back of the source through a long iron pipe and using one of the two spectrometers as a regular beta-ray spectrometer.

During the construction and development of this instrument a new approach in fast coincidence techniques was developed, namely the "time-to-height converter" method of analysis.[7,8] Although not in the original plans, this innovation was used and incorporated in the coincidence circuit with much success.

Usually multipolarities of transitions are determined from their conversion-electron coefficients, relative intensities of the conversion electrons, angular correlation of the emitted particles and/or gamma rays, or, if measurable, the lifetime of the state.[3] With this coincidence electron spectrometer it is hoped that uncertainties in the energy levels of excited nuclides can be explained, not only by reliable coincidence measurements but also by giving limits to the lifetime of the state being investigated and, in one way or another, assigning the multipolarity of the transitions.

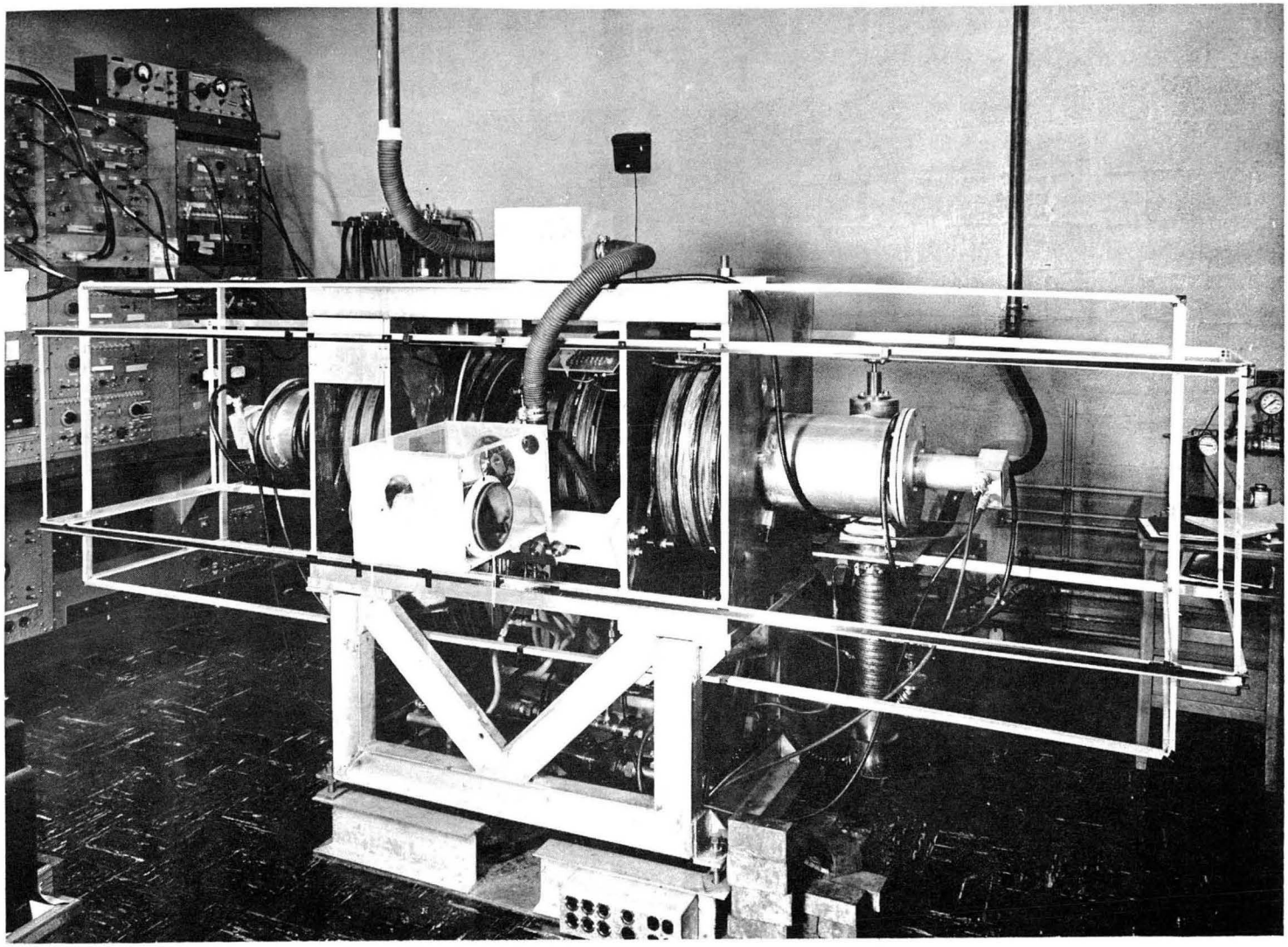

ZN-1694

Fig. 1. Electron-electron coincidence spectrometer.

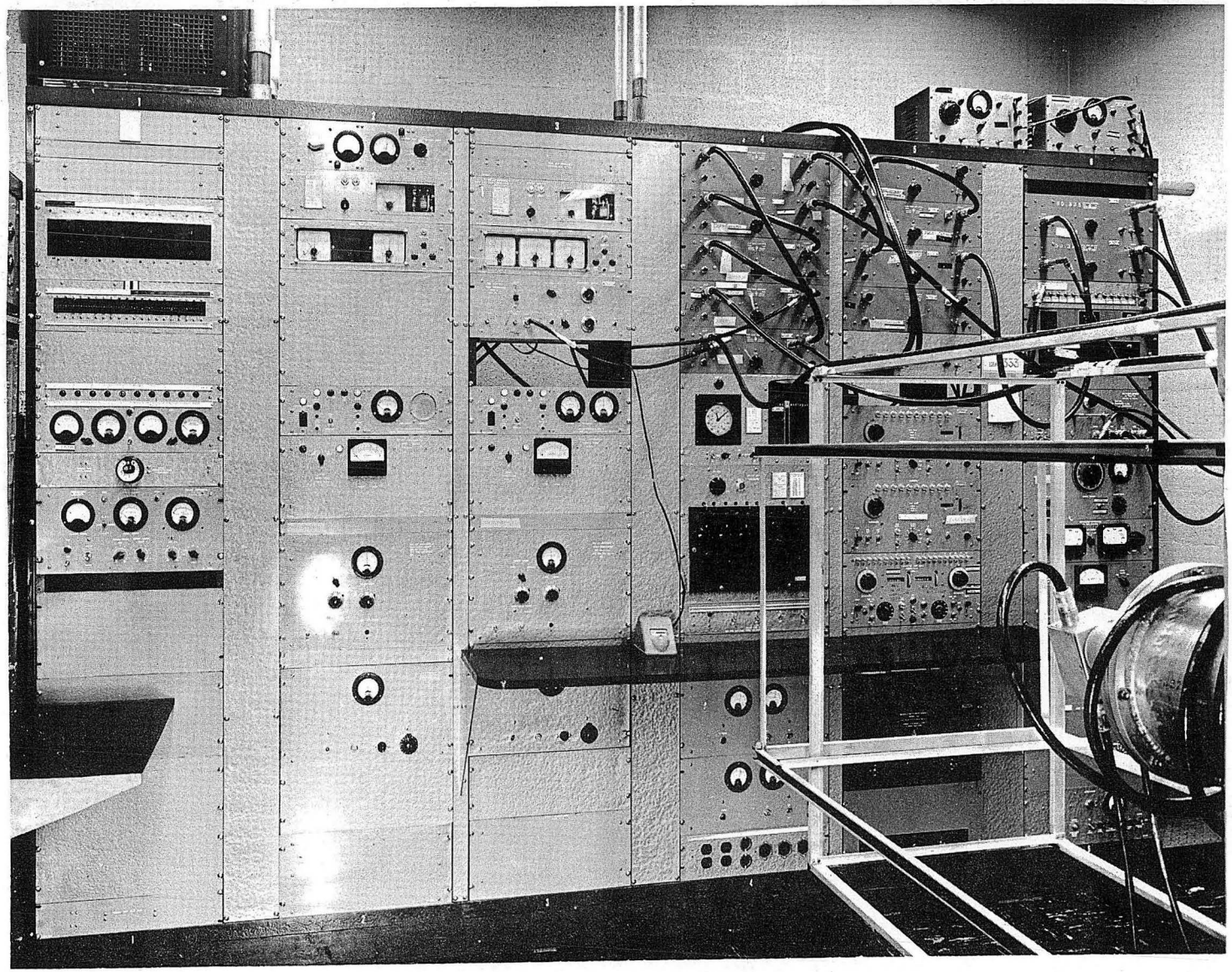

ZN-1696

Fig. 2. Control and counting panel for the electron-electron coincidence spectrometer.

B. DESCRIPTION OF THE SPECTROMETER

1. Spectrometer and Vacuum Tank

The vacuum tank, the two magnetic coils, the two trimmer coils, and the Helmholtz pair coils are all supported by a welded frame of aluminum alloy angles and channels that is 50 in. long, 27 in. wide, and 62 in. high. The magnets are suspended from the top by a centrally located 1-in.-thick aluminum sheet, and the vacuum chamber is supported by the vertical 1/2-in.-thick sheets with brass screws.

The vacuum chamber is made of rolled 0.125-in.-thick 61 S-T aluminum alloy sheet shaped into a cylinder with a mean diameter of 9.6 in. and aluminum-welded together at the edges. Its over-all length is 200 cm and it is divided into three sections: the left spectrometer tank, the sample or source tank located at the center, and the right spectrometer tank. (See Fig. 3.) Such a division makes adjustments easier, and in case of contamination only the source tank would have to be replaced. These three parts are joined together by nonmagnetic stainless steel bolts and nuts, and with the use of rubber gaskets and Celvacene heavy vacuum grease,* a vacuum of 10^{-5} mm of mercury is easily attained. The left and right tanks, which are two independent spectrometer chambers, are supported at each end by three brass screws mounted on the main stand of the instrument. This permits adjustments to be made on the position of the vacuum tank in relation to the magnetic field.

Discs of 0.5-in.-thick brass are bolted, with rubber gaskets, to each end of the spectrometer; to these are attached the detectors to be used in a given experiment. There are three types of end plates corresponding to the three detectors that can be used with the spectrometer. Thus, by changing end plates, a different counter can be used with the spectrometer.

The sample is introduced through an air-lock assembly located at the side of the center section by a highly polished nonmagnetic stainless steel probe, 0.77 in. in diameter and 12.4 in. long. To insure the safety of the operator of the spectrometer, a lucite glove

* This vacuum grease is made by Distillation Products Industries, Division of Eastman Kodak Co., Rochester, New York.

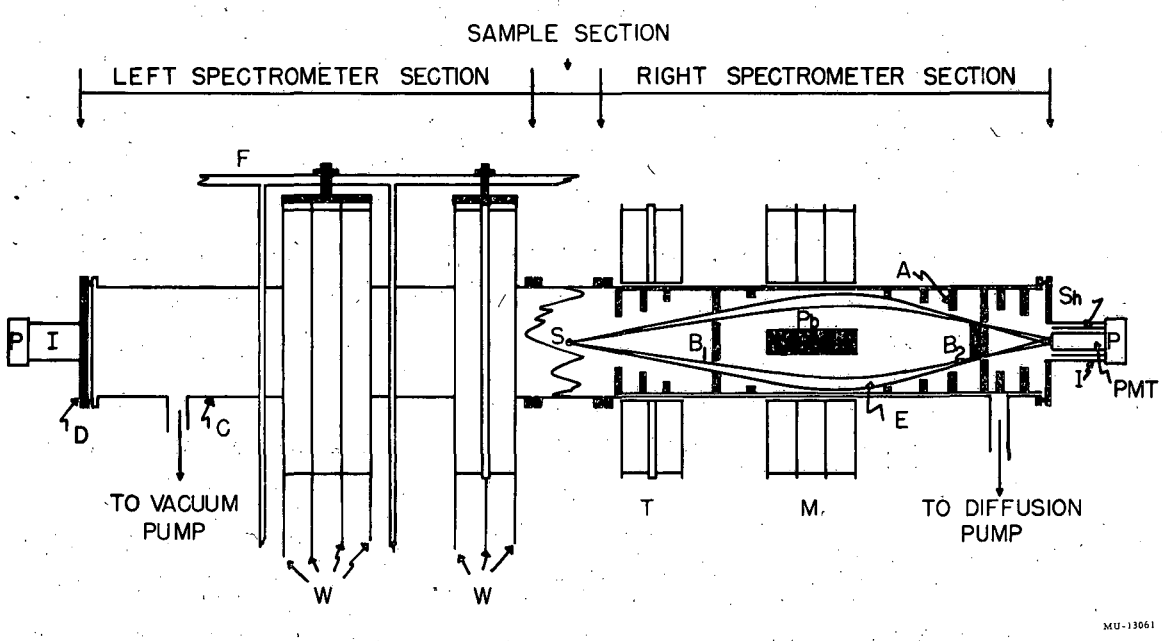

Fig. 3. Longitudinal section of the electron spectrometer.

LEGEND FOR FIG. 3

Fig. 3. Longitudinal section of the electron-electron coincidence spectrometer.

M - main magnetic coils
S - source
B_1 - first aluminum baffle
B_2 - ring-focusing baffle
Pb - lead baffle for gamma rays
T - trimmer coils
A - aluminum baffles to reduce electron scattering
D - scintillator
PMT - photomultiplier tube
SL - mu-metal-shell magnetic shield
F - spectrometer frame
C - vacuum tank
E - approximate electron path
P - preamplifier and cathode follower
W - water cooling tubes
I - iron photomultiplier-tube shield
D - end plate

box was clamped to the center section of the spectrometer at the source entrance. The sources are mounted onto the probe inside this box, which is connected to an air filter and to the building ventilation system. This arrangement lessens the danger of spilling or dropping the sample, especially with sources mounted on thin plastic films, which easily break when a gush of air hits them or simply become brittle and crack after a while.

2. Vacuum System

The vacuum equipment of the spectrometer consists of a Kinney* (Model KC-5) vacuum pump as the roughing pump and an oil-diffusion pump with a Duo-Seal** vacuum pump as the fore pump. Since no magnetic parts were allowed within a radius of two meters from the instrument, the diffusion pump had to be built out of nonmagnetic stainless steel in order that it could be attached directly to the vacuum chamber. The barrel is 14.5 in. long and 4.0 in. in diameter. The cooling tube is a 0.25-in.-diameter soft copper tube soft-soldered around the outside of the barrel with a pitch of 0.6 inch. Laboratory tap water is used at the rate of 1 gal per min to cool the diffusion pump. The jets for the pump were obtained from commercial diffusion pumps and Distillation Product's No. 20 diffusion oil is used in the pump. Since the installation of the spectrometer, no maintenance of the vacuum pump has been necessary.

The spectrometer tank can be pumped down to 10^{-5} mm of mercury from atmospheric pressure in about an hour. The building vacuum outlets are used for preliminary evacuation of air, i.e., from 1 atmosphere to about 2 in. of mercury, then the roughing pump carries it down further to about 80 μ. It has been the practice to use the diffusion pump with the roughing pump for pressures of 80 to ~ 20 μ. From 20 μ down, the diffusion pump is used alone. Tank vacuum is measured by a type-501 thermocouple vacuum gauge*** and an RCA-1949 ion gauge.

---

* Made by Kinney Manufacturing Division, Boston, Mass.

** Made by W. M. Welch Scientific Co., Chicago 10, Illinois.

*** Made by National Research Corporation, Equipment Division, Newton Highlands 61, Mass.

It was observed that some oil vapor from the diffusion pump escaped into the spectrometer chamber, where it finally condensed on the inside walls. To prevent this a double Venetian blind type of baffle, one section on top of the other, was placed between the diffusion pump and the vacuum chamber as an oil trap. Originally copper tubes were soldered on the trap's walls for cooling either by liquid freon or by tap water. Further cooling of the trap was found unnecessary, however, for air cooling was sufficient. The installation of the oil trap was found to hamper the pumping capacity of the diffusion pump only slightly, but it completely prevented the escape of the oil vapors from the diffusion pump into the spectrometer proper.

3. Baffle System

Four types of baffles were used for different purposes (Fig. 4). The first was 30.3 in. from the source and accepted a solid angle between 7° and 10°. This is made of 0.5-in.-thick aluminum disc. The design was based on the calculation by Pratt et al.[5] on the solid angle giving the highest transmission possible for a resolution of 2%. Eight baffles, all made of aluminum, were placed between the first and the ring-focusing baffles. Their function is to reduce the amount of scattered electrons hitting the detector. At the middle of the spectrometer is centrally placed a lead cylinder 8 in. long and 2 in. in diameter enclosed in a 0.125-in. brass shell. This was sufficient to stop the gamma rays from the source from hitting the detectors. A ring-focusing baffle is mounted 6 in. from the detector, where the constriction of the electron beam was determined by photographic techniques to be present. All these baffles are mounted on three brass rods by brass screws so that they can easily be removed and put back into the spectrometer chamber by just pulling the whole baffle assembly. This is found to be very convenient because it is difficult to reach the end of the spectrometer close to the sample from the detector end, a distance of 100 cm and a diameter of only 9.5 inches. In addition, it simplifies the changing of the spectrometer from an electron-electron coincidence spectrometer to an electron-gamma coincidence spectrometer, or vice versa.

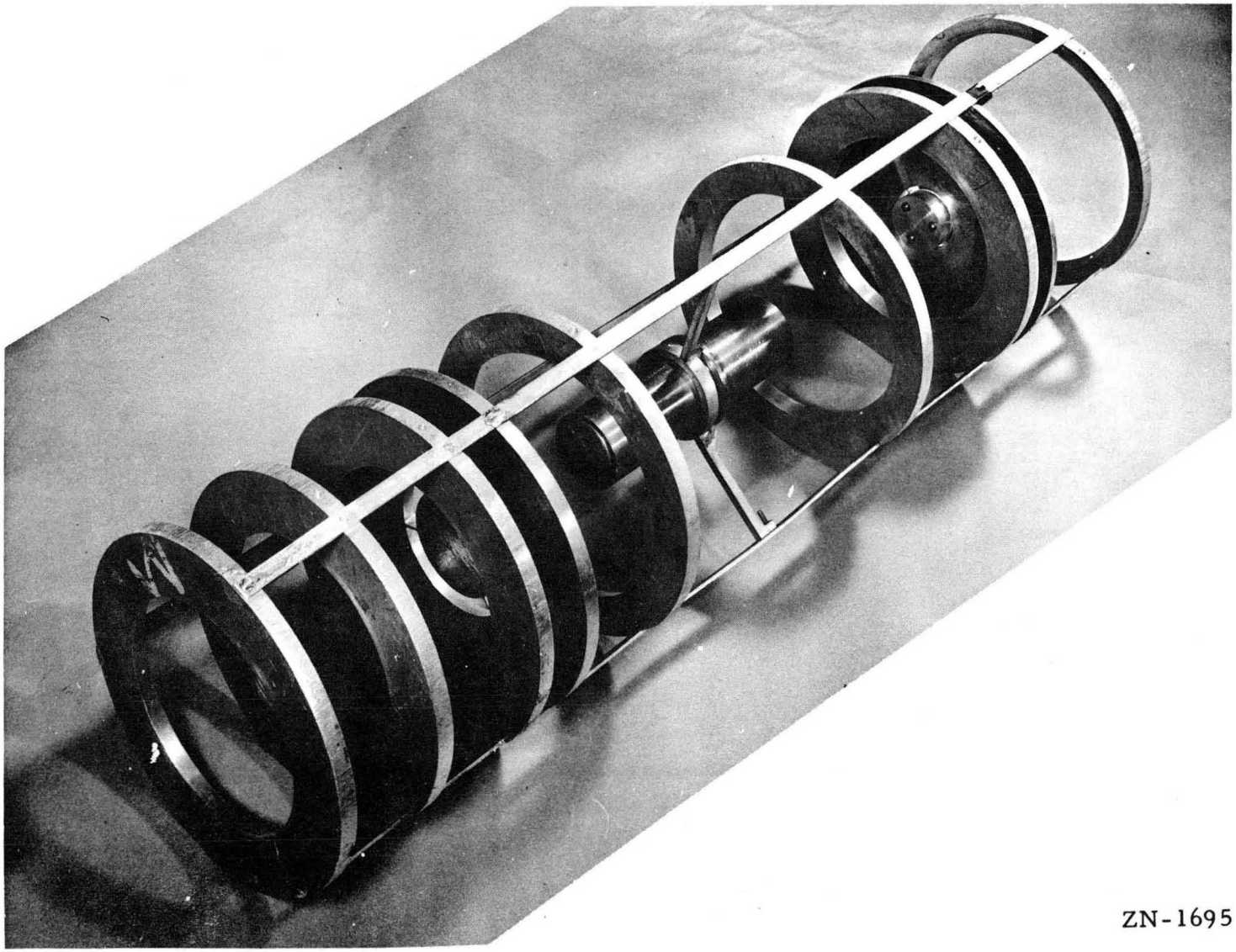

ZN-1695

Fig. 4. Spectrometer baffle system.

4. Magnetic Coils

a. Main coils

The main magnets were designed to be able to focus electrons up to energies of about 3 Mev. With an average radius, $\bar{a}$, of 7.87 in. for the magnetic coil, and a focal length, f, of 10 in., and using the formulas of Deutsch et al.[9] 34,950 ampere turns would be required to focus a 3-Mev electron. The main magnet was constructed with an outside diameter of 20.65 in. and an inside diameter of 10.75 in. To facilitate cooling it was divided into three sections each 1.75 in. wide and 5 in. thick. The spool was made of brass and the inside bottom and sides were covered with a layer of 0.012-in. silicone-bonded glass cloth before No. 11 AWG triple-Formvar-coated copper wires were wound at random simultaneously on the three sections. Approximately 950 turns were wound per section of the magnet, with a resistance of 4.94 ohms per section and with a total resistance for all sections of 14.82 ohms. Thus a total of 2.2 kw is required from the 5-kw amplidyne generator to focus 3-Mev electrons, which leaves enough power for the trimmer coil.

A tap was made on the magnet coil after winding about 790 turns, or more accurately, 3.88 ohms resistance per section. This is advantageous for cases where electron energies of about 1 or 2 Mev are being studied, since the magnet coil is thinner and the danger of inhomogeneity of the magnetic field is less acute. However, the amplidyne generator has to supply 2.6 kw instead to focus the 3-Mev electrons if only 790 turns are used. Hence there are two terminals in addition to the common lead. Terminal connection 2 corresponds to 3.88 ohms, and connection 3 to 4.94 ohms per section. This investigation used only the 3.88-ohm part of the magnet, which was quite sufficient to give satisfactory results with up to about 2-Mev electrons. For very-high-energy electrons, which may be studied in the future, the 4.94-ohm section could be used. A simplified drawing of the main magnet is shown in Fig. 5a.

During the winding of the copper wires, No. 30 iron-constantan thermocouple wire, which is a solid wire wrapped with a double thickness of glass fiber, was imbedded at the center of each section after half

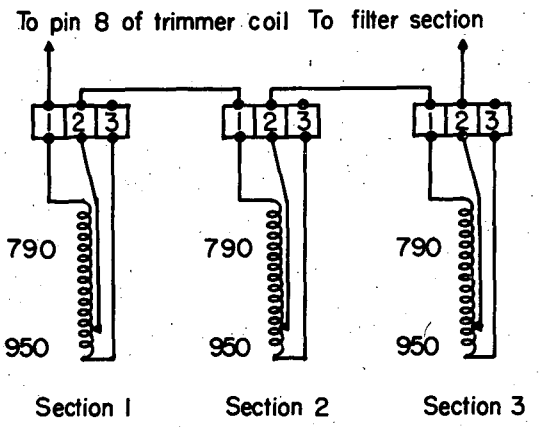

Fig. 5a. Simplified wiring diagram of the main magnet coils, showing the number of turns.

of the wire length had been wound. This wire was then connected to the temperature-protection relays of the power supply. The small amount of iron in these wires is not enough to distort the magnetic field of the spectrometer.

On both sides of the spool and sandwiched between the three sections, 0.25-in.-diameter copper tubes for water cooling purposes are soldered 0.437 in. apart to the brass plates of the magnet. There are four sets of seven tubes each per magnet. Each tube is continuous and has its own intake and outlet connection to the main water supply so that in case one solid tube is plugged, only that single tube would be affected, leaving the rest functioning.

The coils were wrapped outside with a layer of half-lapped glass tape, and the whole magnet was vacuum-impregnated with silicone varnish and baked in the oven. The total weight per magnet amounted to 450 lb. A high-potential test at 1500 volts from coil to ground was applied to the magnet coils to check them for current leaks before they were used.

b. Trimmer coils

In instruments of this type it has always been the objective to make the two joined spectrometers independent of each other; this means that the magnetic field of one should not interfere with that of the other. The conversion-electron peak should be a function only of the current in the spectrometer where it is being detected, and not a function of the current intensity of the other spectrometer. This is important, because one side should always be detecting a certain particular energy while we sweep the whole beta spectrum with the other spectrometer. If the spectrometer were made of iron, this corrective measure would not be necessary, but it must be considered for this nonferrous instrument. There are two ways of solving this problem. One is to increase (or decrease, as the case may be) the magnetic field of the gate side to compensate for the shift in the conversion-electron peak as the magnetic field varies on the other side. Although compensation is usually automatic, it is inconvenient because the current-calibration factor is a function of the power supplied to the opposite magnet. Another approach, which is used in this instrument, is to place compensating or trimmer coils between the two main magnets with the

hope that they will minimize these undesirable disturbances in the magnetic-field distribution as much as possible without distorting the conversion-electron line shape. Since the exact number of ampere turns needed by the trimmer coils to neutralize the effect of the main magnet on the other side of the instrument is not known, the trimmer coils were designed so that one can vary the number of turns to be used from 25 to 1100 turns simply by connecting the proper tap leads located at the outside of the coils. A simplified drawing is given in Fig. 5b.

The trimmer coils are made up of two sections; one has a fixed number of turns, and the other can be tapped at different parts of the coil. The spool is made of brass, with an outside diameter of 20.6-in., an inside diameter of 10.75-in., a total thickness of 5.25 in. and an inside channel width of 1.30 in. per section. Cooling is accomplished by passing water through copper tubes soft-soldered to both sides of the spool as well as through the 0.5-in. thick center cavity between the two sections. The water inlet is at the lower end of the magnet; the outlet leaves the coil at the top end. The same cooling water supply is used for the trimmer and the main magnet coils.

Section 1 of the trimmer coil was wound with 550 turns of No. 9 AWG heavy Formvar-coated copper wire after the inside of the spools were covered with glass tape and 12-mil combination electron "300" insulation. For Section 2 of the coil the same procedure was followed, except that taps were made at 0, 25, 50, 125, 275, and 550 turns by phos-copper-soldering 3/8-in. wide No. 18 B.and S. gage copper strips to the wire. These leads were wrapped with Mylar tape connected to the terminal strip outside the coil. After the coils were wound, they were wrapped on the outside with a half lap of glass tape, vacuum-impregnated with "Dolph - B.C. 307" varnish, and then baked in an oven at 150° C for 8 hours.

5. Cooling System

Because a large amount of magnet current is needed to focus the higher-energy electrons , air-cooling alone is not sufficient to maintain the temperature within optimum range. In addition, the temperature could reach a point where it would ruin the magnet, especially when focusing very-high-energy electrons (~ 2 Mev). For example, a current of 10 amp in a magnet without water cooling increases the magnet temperature

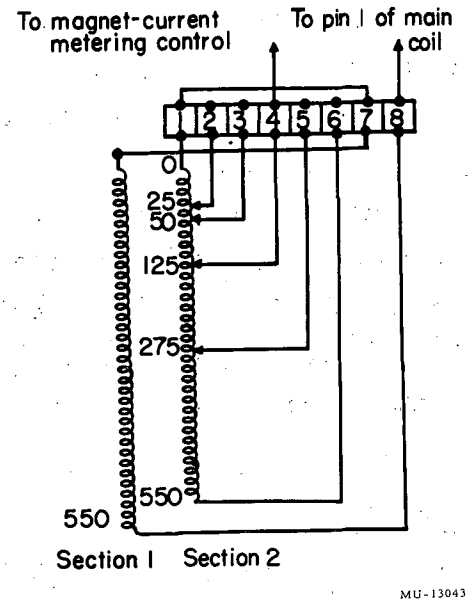

Fig. 5b. Simplified wiring diagram of the trimmer coils, showing the number of turns.

about 2 deg. per min; after 20 min, destructive burning of the coil may occur. When the coils are cooled with water, a current of 15 amp in the coils for several hours causes an increase of only 1° C in the water temperature and 3° C in the magnet temperature. The magnets are cooled by passing "Calgon"* - treated water, which is filtered by a "Micro-Kleen" filter,** through the cooling tubes at a rate of 4 gpm. Water thus treated is used at the University of California Radiation Laboratory for cooling the magnets of the Bevatron, cyclotron, and other accelerators. After use, the water is cooled, the pH is adjusted, and the water is treated and recirculated through the system. To cool the machines adequately with a smaller volume of water, cooling of the water to about 5° C is planned.

The pressure of the water before entering the filters was 40 psi, but dropped to 10 psi after passing through the filters and magnet-cooling coils. To protect the coils in case of water failure, a "Shur-Flo"*** automatic interlock relay, which turns off the magnet current when water flow is below 4 gpm, was placed before each of the magnets.

6. Magnet Power Supply

The two spectrometer units have similar independent magnet power supplies; thus the following description applies to either of the two spectrometers. A block diagram of the magnet current supply is shown in Fig. 6. The magnetic coils obtain their power from a General Electric anplidyne generator, model 5BY1543, which delivers 20 amp at 250 v. This is belt-driven by a Fairbanks-Morse induction motor type QZK, which is rated at 2890 rpm with a full load. Three of the four amplidyne windings were used, with the first two connected in series. The three windings are designated respectively as the reference field, voltage control field, and the anti-hunt field windings. The dc output of the amplidyne is filtered by a filter section to remove some of the ripples present that are caused by the

* Sodium hexametaphosphate, made by Calgon, Inc., 1943 Hagan Bldg., Pittsburgh, Pa.

** Model 3AXB2, manufactured by Cuno Engineering Corp., Meriden, Conn.

*** Made by Hays Manufacturing Co., Erie, Pa.

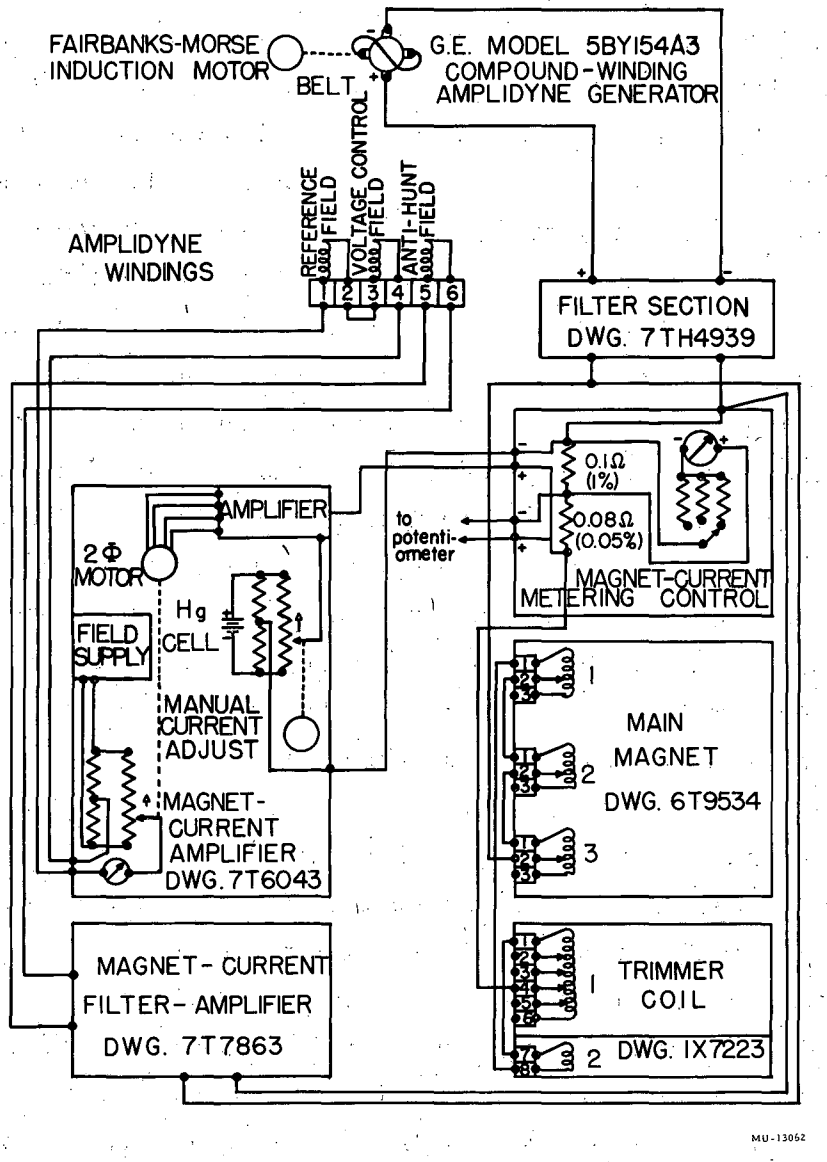

Fig. 6. Magnet-current block diagram.

noise from the brushes and armature of the generator. In series with the dc output is the magnet-metering section where a 0.08000 ± 0.00004-ohm manganin temperature-independent-type resistor and a 0.1000 ± 0.0001-ohm precision wire-wound resistor are used to measure the current going to the magnet. A Rubicon No. 2780 potentiometer, standardized against an Epply No. 100 standard cell using a Leeds and Northrup type 2420C galvanometer, determines the potential drop across the manganin resistor, while a direct-reading ammeter with ranges 0 to 1, 0 to 10, and 0 to 25 amp is connected to the 0.1000-ohm resistor. After being filtered and measured, the current goes to the magnets. The main and trimmer coils are connected in series and with opposing magnetic fields.

To stabilize the power in the magnetic coils, the potential drop across both the 0.08000- and the 0.1000-ohm resistor of the magnet-metering section is fed into the magnet-current amplifier where it is continuously compared to the potential supplied by four mercury cells spot-welded together. The amount of reference potential from the mercury cells is determined by connecting a 5000-ohm Helipot resistor to the manual current control. Any excess unbalance current between the reference potential and the potential drop across the resistors of the magnet-metering section is detected and amplified by a Leeds and Northrup amplifier. The amplifier sends correcting signals to a 2-phase motor which is connected through a clutch to a 100-ohm Helipot resistor that controls the field current being fed to the reference and voltage-control amplidyne windings. Hence, any increase or decrease in the current output of the amplidyne would be detected by the amplifier and would result in the decrease or increase of the amplidyne field current until the normal current output is obtained. With this arrangement, variations in current of up to 9 cps are corrected. For fluctuations of from 9 to 60 cps, the filter amplifier section of the dc power supply to the magnet can compensate within a second. In this setup, no precaution was deemed necessary for stray pulses greater than 60 cps because such high-frequency noise is essentially short-circuited by the large capacitors located in the magnet-current filter amplifier.

Examination of a circuit consisting of the amplidyne, magnetic coils, and damping condensers showed that a resonant frequency of

9 cps was present along with a 60-cps noise, and the system was not at all stable. To remove both the weak 60-cycle and the strong 9-cycle disturbances in the amplidyne output, a part of the dc output of the amplidyne with the 60-cycle noise is tapped at the filter section and inverted by a transformer. When this inverted 60-cycle signal is mixed with the regular field-current supply, the original 60-cycle noise is cancelled, leaving only the strong 9-cycle resonance. This is amplified at the filter amplifier of the magnet-current supply and fed into the anti-hunt field winding of the amplidyne 180° out of phase by inverting the leads. With this arrangement, the resonant-frequency noise and the 60-cycle signal picked up from the nearby ac cables were eliminated.

A test for stability was made by connecting the potentiometer output to a Leeds and Northrup Speedomax recorder. With a current of 4 amp, enough to focus a 600-kev electron, the noise or ripple was 0.25 mv, equivalent to 3 ma. This is better than 1 part in 1000 current control. After the magnet was operated for 17 hr, the observed shift was 25 ma, which is a current regulation of 6 parts in 1000. Most of the power shift occurred during the first hour when the magnet was still cold. Thereafter a current regulation of 3 parts per 1000 was achieved. No marked increase in temperature was noted from the thermocouples in the magnet.

7. Earth's-Field Compensating Coils

For air-core spectrometers with long electron paths like this one, transverse components of the earth's magnetic field need to be cancelled out, especially for low-energy electrons. If no compensation is made for this factor, the transmission drops down as the electron energy decreases because the earth's field pulls the electrons out of focus. In addition, deviations in the current-calibration constant are observed. It was decided to follow Haynes and Wedding's[10] method in designing the rectangular coils (Helmhotz pair coils) to neutralize the earth's field inside the spectrometer.

Two vertical frames each 129 in. long and 36.5 in. high and two horizontal frames each 139 in. long and 26.5 in. high were made from 1-by-0.5-in. aluminum alloy channel. These were attached to the

framework of the spectrometer with brass screws so that the vacuum chamber was boxed by the four rectangular frames. On each of the vertical frame pieces was wound in series 125 turns of No. 26 Formex* copper wire coated with heavy Formvar. This is the horizontal component field coil. In each of the horizontal frames, which is the vertical component, was wound 250 turns of No. 26 Formex copper wire. Power for these coils was obtained from two standard regulated power supplies.

To almost completely neutralize the magnetic field effects on the low-energy electrons, the Helmholtz coils should be supplied with precise amounts of currents. An ordinary magnetic compass is not sufficient to detect the null point while the current intensities of the horizontal and vertical coils are varied, so a 5-in. RCA-5CP1A cathode tube with a variable control for the electron energy produced by the electron gun was placed at the center and along the axis of the spectrometer chamber. It is assumed that when electrons of about 800 kev are accelerated by the electron gun, they are not affected by the earth's field; hence their luminescent spot on the oscilloscope screen was made the fiducial mark for a cancellation of the earth's magnetic field at the center of the chamber. The accelerated potential was decreased to a few kv, and the bright spot was displaced about 1.5 cm. When the power supplied to the Helmholtz coils was adjusted the bright spot was brought back to its original position. With this current setting, the energy of the electron was again varied from 800 kv to a value as low as possible before the luminescent spot began to spread, and no noticeable shift in its position was observed. The current required was 75.8 ma and 57.8 ma for the vertical and horizontal coils respectively.

8. Electron Detectors

For counting electrons, a highly polished circular disc of Livermore plastic scintillator** 0.5 in. in diameter and 1/8 in. thick was optically bonded to the center of a 1/8-in. lucite circular

---

* Made by Formex Wire Company, Anaheim, California.

** This plastic scintillator is composed of styrene with 2.5% terphenyl, 0.03% tetraphenyl butadiene, and 0.01% zinc stearate.

plate 2 in. in diameter by Biggs' bonding agent R-313.* With this arrangement, the lucite rested on an O-ring at the end plate of the spectrometer chamber, with the plastic scintillator side in vacuum. Optical contact between the lucite and the RCA-6655 photomultiplier-tube window is provided by white petrolatum.** The photomultiplier tube was shielded from the magnetic field by a mu-metal shell and an iron tube screwed to the end plate of the spectrometer chamber, and the cathode-follower housing provided the necessary support as well as light protection. For cases where electrons of less than 60 kev are being studied, Harshaw anthracene crystals of the same size are used instead of the plastic scintillators. Usually a 1000-v potential was applied to the photomultiplier tubes in all the experiments.

In experiments where low-energy electrons are being studied and no coincidence measurements are to be made, the end plate of the spectrometer containing the side-window G-M counter can be used. The G-M counters are made of brass and the thin plastic windows are supported by grids.[11] VYNS-3 films were used as counter windows, which allowed detection of 1-kev conversion electrons. A mixture of 90% argon and 10% ethylene was used in the counter.

9. Coincidence Circuit

The negative pulses of the "start" side of the coincidence circuit are sent from the photomultiplier tube through a preamplifier and cathode follower to a bank, usually three, of Hewlett-Packard 460A wide-band amplifiers (modified).*** After the first wide-band amplifier, the output pulses, still negative, are branched. One part goes to a UCRL linear amplifier and then to a 1024 scaler, while the other part is further amplified by more wide-band amplifiers until all the pulses are saturated. Finally, the negative output of the last Hewlett-Packard 460A unit is fed into the "start" input of the time-to-height converter. (See Fig. 7.)

* Bonding agent R-313 by Carl H. Biggs Co., 2255 Barry Avenue, Los Angeles 64, California.

** White Protopet No. 1 (Petrolatum U.S.P., White) by L. Sonneborn Sons, Inc., New York City, N. Y.

*** Hewlett-Packard Co., Palo Alto, California

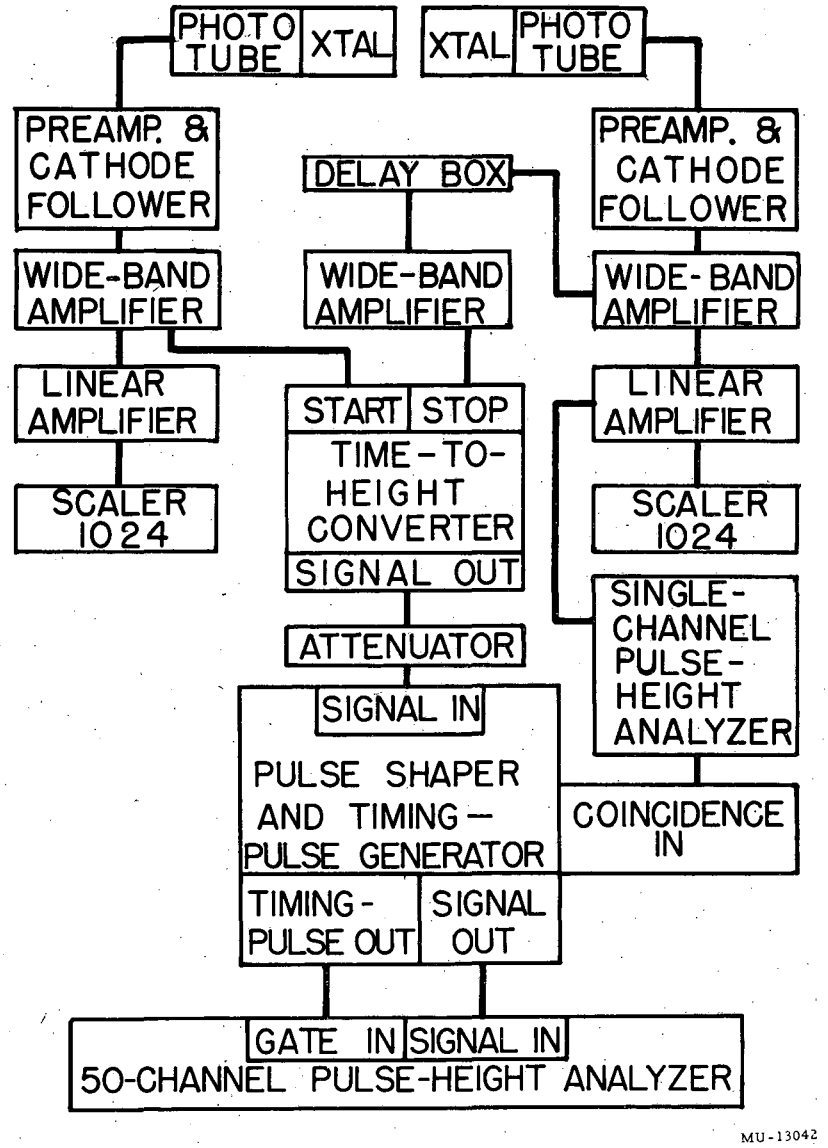

Fig. 7. Fast-slow coincidence-circuit block diagram.

On the other hand, the pulses from the "stop" side of the circuit, after being amplified by a 460A wide-band amplifier, then go through a 460B wide-band amplifier to a delay box consisting of measured lengths of RG-63/U or Amphenol 21-342 cable.[12] From the delay box the pulses, now positive, are fed to another 460B amplifier where they are further amplified and converted to negative pulses. From the last 460B wide-band amplifier, the pulses are fed to the "stop" input of the time-to-height converter, whose output pulse is proportional to the time interval between the "start" and "stop" pulses.

Because the output of the time-to-height converter is a negative pulse, it must be converted into a type that can be used in the 50-channel pulse-height analyzer. Thus, the output of the time-to-height converter is attenuated and then fed into a Los Alamos DD2 linear amplifier[13] whose output is a positive short pulse. This pulse is sent to the pulse shaper, where it is stretched to about 10 μsec, and fed into the input of the 50-channel pulse-height analyzer.[14]

To reduce the chance coincidences, a slow-coincidence circuit was used. One of the outputs of the UCRL linear amplifier on the "stop" side of the circuit was connected to the input of a Los Alamos-type single-channel pulse-height analyzer. The pulses above noise from the analyzer are fed into the "gate" part of the slow triple-coincidence circuit of the pulse shaper and timing-pulse generator. Here a part of the signal or start pulse triggers a multivibrator, which sends its pulse to the triple-coincidence circuit. Only when the pulses from the start pulse and the gate pulse arrive within resolving time of the circuit, about 2 μsec, will a timing pulse be generated. This is used as the gate pulse for the 50-channel pulse-height analyzer.

10. Sources

Sources are made by evaporating 5- to 20-λ solutions of the sample on 0.1- to 0.5-mil copper, gold, platinum, or plastic films, depending on the sample and the experiment. These backings are mounted on a brass ring, 0.5 in. in diameter, soldered to a brass rod, which inserts into the sample probe end. From the author's experience, metal foils are more convenient than plastic films, and there is less danger

of charging in the source even when the films are painted with Aqua-Dag. The effect on the peak is to broaden its shape (poorer resolution) and to decrease its counting rate (lower transmission). However, these are minor points compared to the ease in using metal foils. Nevertheless, for low-energy electrons, thin films have to be used. After different plastic films were tried "VYNS-3" * (a polyvinylchloride-acetate) was chosen over "Zapon", "Tygon", or "Clear Clad No. 1060".[11] Usually two layers of film with a total thickness of 10 to 20 $\mu g/cm^2$ are used for source backings. VYNS resin, a finely ground white powder, was dissolved in cyclohexanone, and the film was made in the manner of Pate and Yaffe.[15]

C. TESTING AND OPERATION CHARACTERISTICS OF THE SPECTROMETER

1. Ring-Focusing Baffle

After the spectrometer was assembled and a good vacuum was obtained, an initial run was made using a 1-mC source of Cs^{137}, which was procured from Oak Ridge National Laboratory and mounted on a 1-mil copper foil. The plastic scintillators were each masked by a 0.4-in.-thick aluminum disc having a cone-shaped bore at the center measuring 3 mm at the smallest diameter; this side was placed closest to the scintillator. With only the first aluminum baffle and the center lead shield, the counting rate of the Cs^{137} 625-kev conversion-electron peak was maximized by moving the coils. The purpose of this run was to determine the current necessary to focus the conversion electrons of Cs^{137} so that they would hit the scintillators located at the ends of the spectrometer chamber. Then with the same current setting, a Kodak No-Screen x-ray photographic plate was placed horizontally at the axis of the spectrometer chamber near the detector end and exposed for 20 hr to determine approximately the path of the electrons and also the region where ring focusing occurs. The exact position

* VYNS-3, Blend B-643, made by Bakelite Co., a division of Union Carbide and Carbon Corporation, 30 East 42 Street, New York 17, N. Y.

of the ring focusing had to be determined and could not be based on the findings of Pratt et al.[5] because the presence of the trimmer coils produces a perturbation on the magnetic-field distribution which was not present in the previous investigations. After the expected location of the constriction in the electron path was determined from the above pictures, a series of x-ray plates was exposed at distances 0.25 in. apart in this region. Each plate was exposed for a period of 10 hr with the same sample and current settings. The K- and L-conversion electrons were well defined in all the plates and the position where the K- and L-conversion-electron line widths were smallest and the separation was largest was chosen for the ring-focusing-baffle position. To test the effect of the trimmer coil on the ring-focusing position and, indirectly, the perturbation of the trimmer coil on the main magnetic coil field, a similar experiment was performed without the trimmer coil. Exactly the same results were obtained for both cases, except that a different current calibration constant or factor had to be used to focus the same conversion electrons.

From the results of the x-ray photographic determination (Fig. 8a), an aluminum ring-focusing baffle (Fig. 8b) was designed to accept all the electrons of the same energy. The slight noncircular form of the picture is due to the film's not being held flat during the exposure.

2. Transmission of the Spectrometer

An absolute determination of the transmission of the coincidence spectrometer was made using a Bi^{207} source, which decays primarily through the 569-kev transition. The amount of this transition in the source was 4.15×10^6 dpm and was calculated from the gamma spectrum obtained from the Penco* 100-channel pulse-height analyzer using a shelf geometry of 1.29% and a dead-time correction of 69%. The crystal efficiency curves of Kalkstein and Hollander[16] (using the same NaI (Tl) crystal) were used to calculate the strength of this transition. From the K-conversion coefficient of Wapstra for the 569-kev transition, which is 1.5×10^{-2}, the absolute number of K-conversion electrons

* Model PA-3 made by Pacific Electro-Nuclear Co., Culver City, Calif.

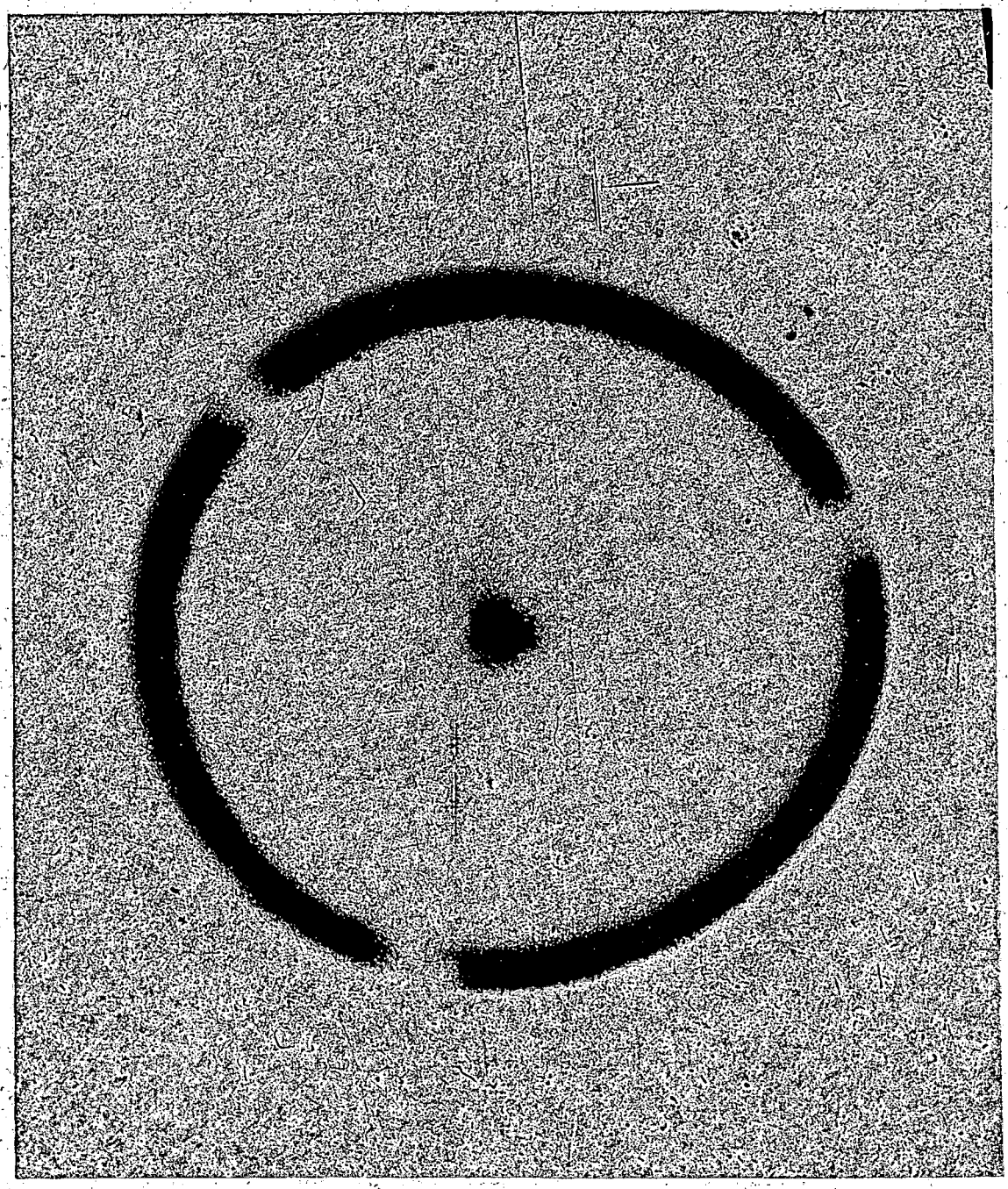

ZN-1693

Fig. 8a. Cs^{137} conversion-electron picture at the ring-focusing position.

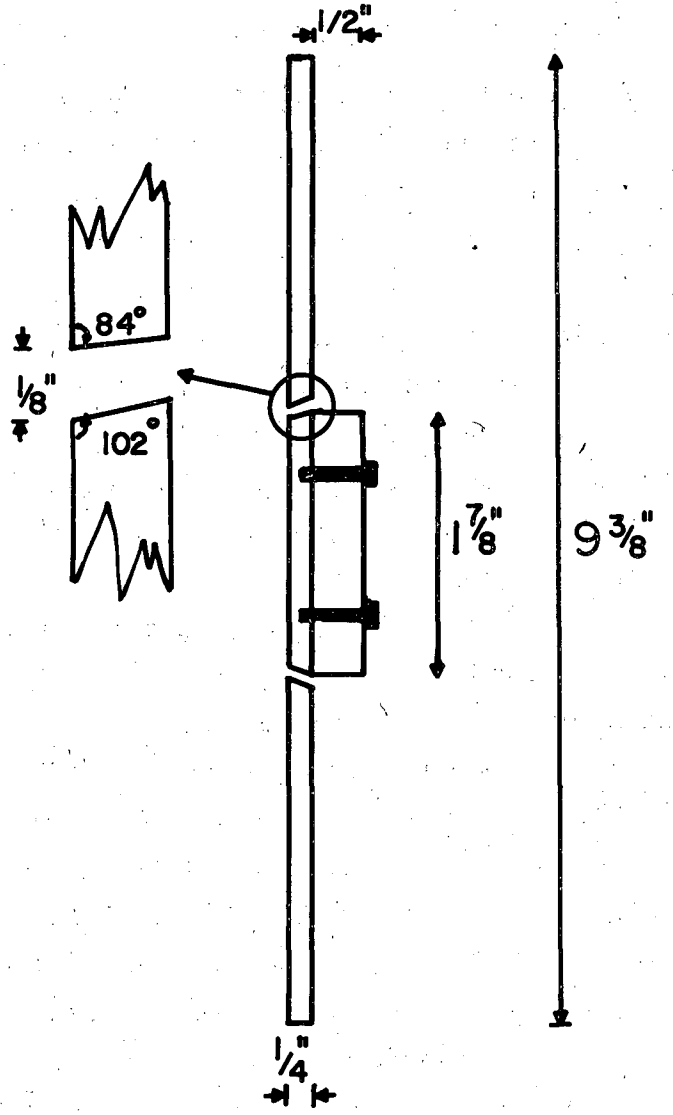

Fig. 8b. Dimensions of aluminum ring-focusing baffle based on Fig. 8a picture.

for the transition was calculated and compared to the total number of electrons detected for the K-conversion line of the same sample. A transmission of 1.0% was obtained for a resolution of 2.3%, which was the transmission expected when the instrument was designed.

3. The Effect of the Trimmer Coil on the Operation of the Spectrometer

With the 624-kev conversion electron of Cs^{137} as the source, a series of beta spectra were studied using different current intensities in the opposite spectrometer magnet coil. The results are shown in Fig. 9 for the cases where no trimmer coils were used while 0, 6, and 12 amp were supplied to the opposite coil. A marked shifting of 11.6 kev/6 amp increase in the opposite magnet was observed even for such high-energy conversion electrons. The low-energy conversion lines like the 37-kev K conversion-electron peak of Am^{241} were not only shifted more, but they were also distorted in shape and also their resolution was poor.

The compensating power of the trimmer coil was determined by using different numbers of the coil, and it was found that 675 turns maintained a sufficiently fixed calibration constant without distortion of the spectral line shape even with 15 amp (enough to focus more than 2-Mev electrons) on the other spectrometer coil. The real test of the trimmer coil was with the 37-kev conversion lines of Am^{241} at different current intensities in the opposite magnet. The results shown in Fig. 10 clearly prove that with the trimmer coil, shifting and distortion of line shape has been reduced to such an extent that they can be considered negligible.

Another test made to confirm the effect of the trimmer coil was to run the complete beta spectrum of Cs^{137} on the other spectrometer both with 10 amp and without current. The experimental points still fell on the same line; the results are given in Fig. 11.

4. Calibration of the Spectrometer

Each side of the spectrometer was calibrated independently using well-known standards such as Am^{241}, Hg^{203}, Tm^{170}, Cs^{137}, and Bi^{207}. As a further check on the calibrations, measurements were made when the magnet was cold, and these were compared with those obtained after the magnet had been operating for more than an hour. In addition,

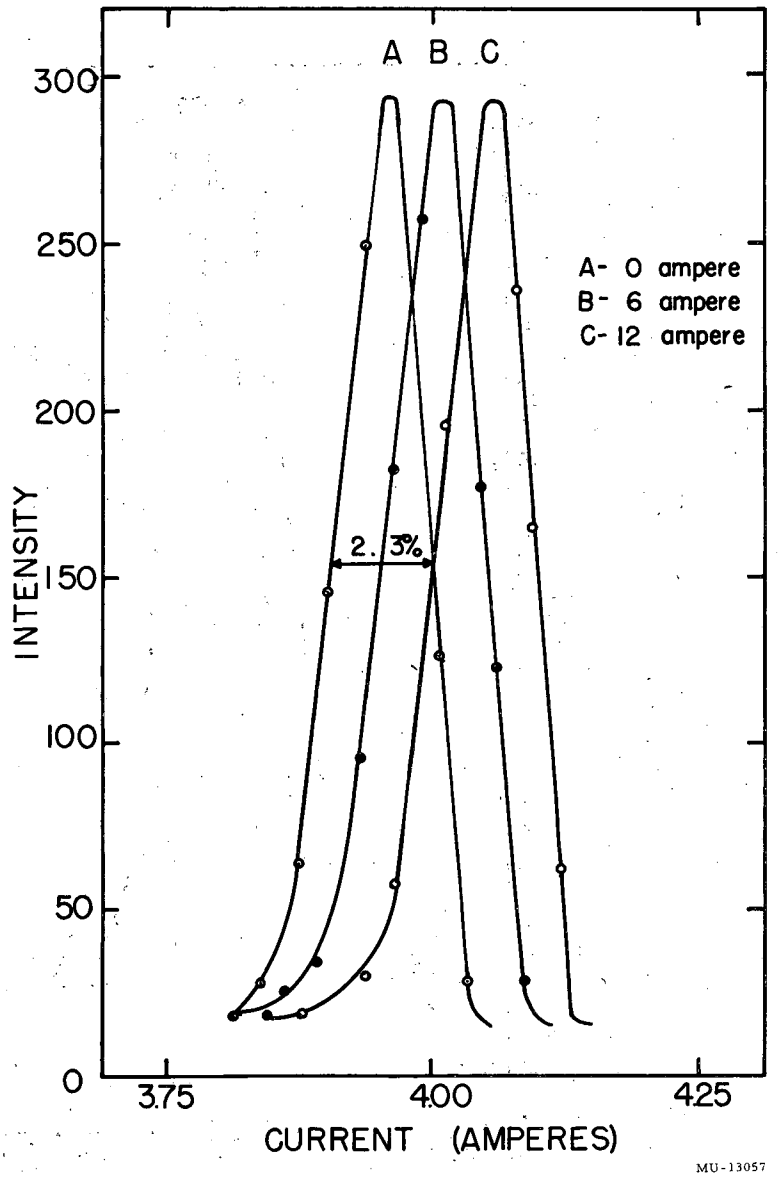

Fig. 9. Effect of the magnetic field on the opposite spectrometer on the Cs^{137} K conversion-electron line when no trimmer coils are used.

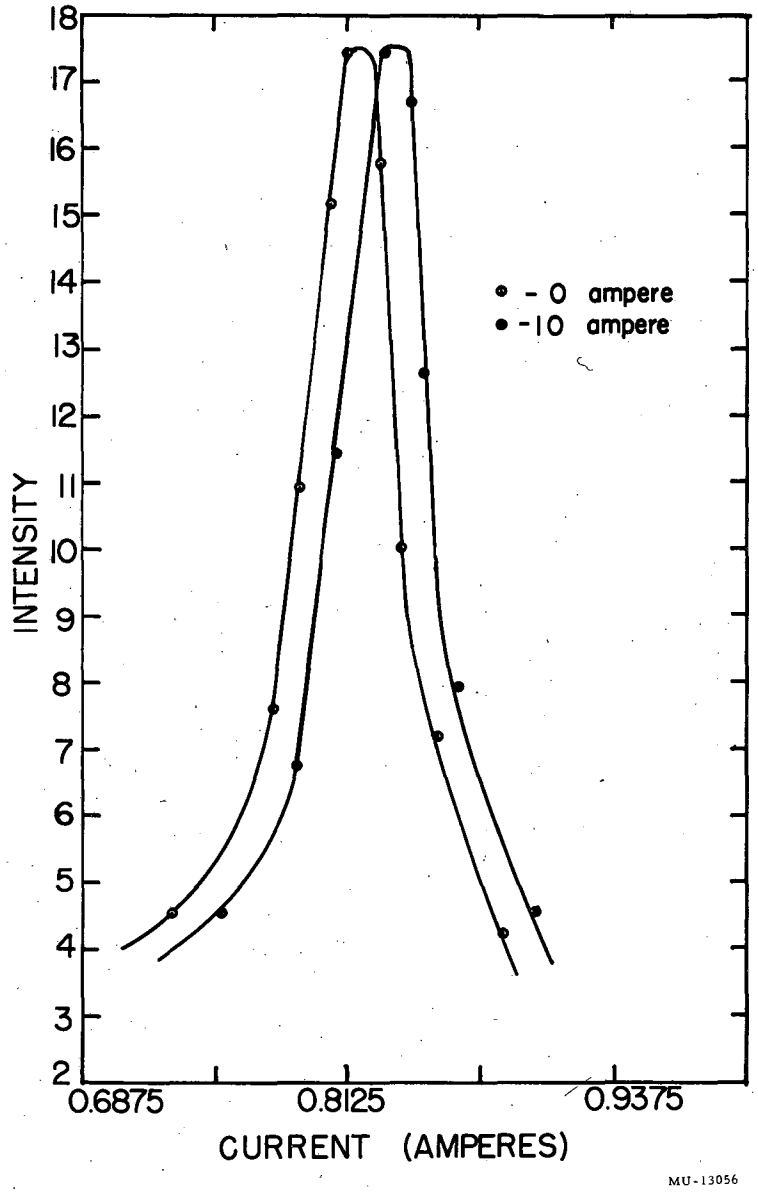

Fig. 10. Effect of the magnetic field of the opposite spectrometer on the L line of the 60-kev transition of Am^{241} with the proper trimmer coils.

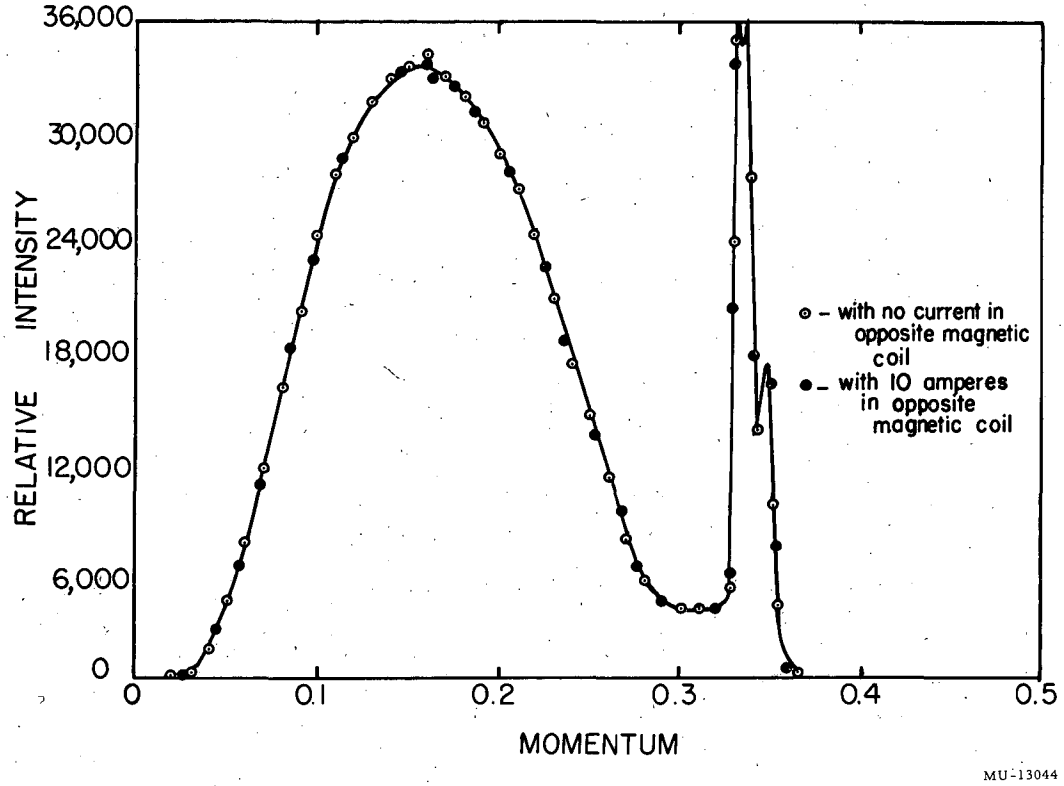

Fig. 11. Compensating effect of the trimmer coils in the opposite spectrometer with the beta spectrum of Cs^{137}.

the spectrometer was also calibrated with the opposite spectrometer turned off and with 16-amp current, the maximum available, supplied to the main magnet coil. In all these, the same calibration constant C was obtained for the equation

$$H\rho = CI = (C\,E)/R,$$

where $H\rho$ is the magnetic rigidity of the electron being focused by the spectrometer;

C is 801.30 gauss-cm per amp;

I is the current being supplied to the main magnet coil, in amp ;

E is the potential drop across R as determined by a potentiometer; and R is a manganin-type resistor known to be precisely 0.08000 ± 0.00004 ohm .

A plot of $H\rho$ in gauss-cm against I in amperes is given in Fig. 12 for some standards used to calibrate the instrument and some other conversion electrons whose energies are known with confidence from precision permanent-magnet electron spectrographs. All the experimental points fall on a straight line and are reproducible. Due to hysteresis, this is impossible for spectrometers made of iron (Table I).

TABLE I

Standard	Transition Energy (kev)	Conversion Shell	Electron Energy (kev)	$H\rho$ (gauss-cm)	Current (amp)	C (gauss-cm/amp)	Reference
Tm^{170}	84.1	K	23.4	521.7	0.651	801.33	17
Am^{241}	59.57	L	37.2	662.1	0.826	801.31	18
Hg^{203}	279.0	K	193.5	1617.7	2.019	801.30	19
		L	263.7	1942.2	2.424	801.29	19
Cs^{137}	661.6	K	624.21	3381.3	4.220	801.28	3
		L	655.6	3498.1	4.366	801.30	3
Bi^{207}	569.0	K	481.0	2836.2	3.539	801.30	20,21
		L	553.1	3113.4	3.886	801.28	20,21
	1063.9	K	976.0	4657.9	5.813	801.32	3,20
		L	1048.0	4913.2	6.131	801.40	3,20

C = 801.30 based on Cs^{137} and Bi^{207}

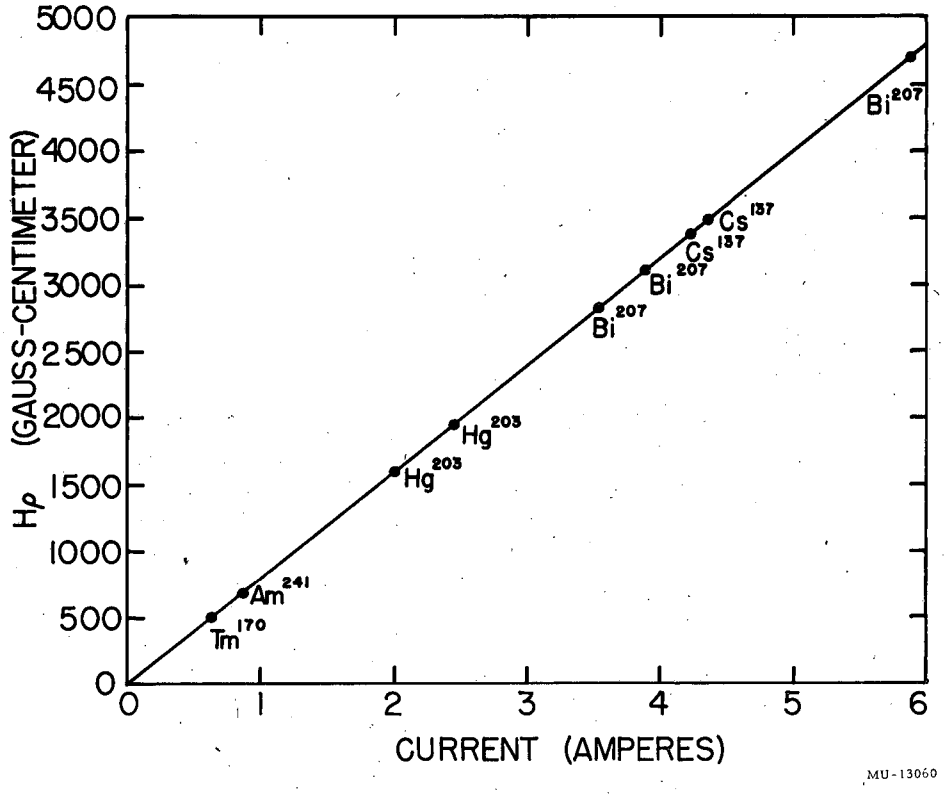

Fig. 12. Calibration curve of the spectrometer.

5. Time-to-Height Converter Calibration

The time-to-height converter, to be written from now on as THC, gives a positive pulse output the height of which is proportional to the time difference between the start and stop pulses. However, it is known that at very short times, of the order of a millimicrosecond, or at very long time intervals, about 5×10^{-7} sec, the linear relationship between the time difference and pulse-height output shows a slight deviation. The term nanosecond,[23] n sec, would be used instead of μsec in the succeeding pages. Therefore to be able to get reliable and accurate results the THC was used in the proper range by introducing an arbitrary fixed delay to the stop pulse. Using the start pulse also as the stop pulse, the THC was calibrated by adding known lengths of cable or known time delays from the delay box to this fixed delay and measuring the height of the output pulse with the 50-channel pulse-height analyzer. A typical calibration curve is given in Fig. 13. By adjusting the amplifier gains a resolution as poor as 10 n sec to as good as 0.5 n sec per channel is easily attained. These peaks are usually two channels wide with maximum widths of three channels. For most purposes the THC is used with 2 n sec per channel so that the peak would be more pronounced and easier to detect since it is less spread. This is true when working with a few coincidence events in the presence of a high background like a continuous beta spectrum.

The main advantage of this type of coincidence analysis is the time element. The whole delay curve is obtained in the same time required to get a point of the curve in the conventional way. This is very helpful for short-lived nuclides. Furthermore, error due to drifts of the instrument is reduced to a minimum.

Although the peaks are only two channels wide during calibration, they are broader in actual experimental conditions. This can be explained by the statistical fluctuation of electron transit times in the photomultiplier tube and in the whole circuit itself. One way to solve this problem is to use photomultiplier tubes having 14 stages or more, like the RCA-6810, where the output can be fed directly into the THC. As long as plastic scintillators or organic scintillators are used the crystal contribution to the broadening of the peak is negligible; however, for crystals like NaI(Tl) which are slow crystals

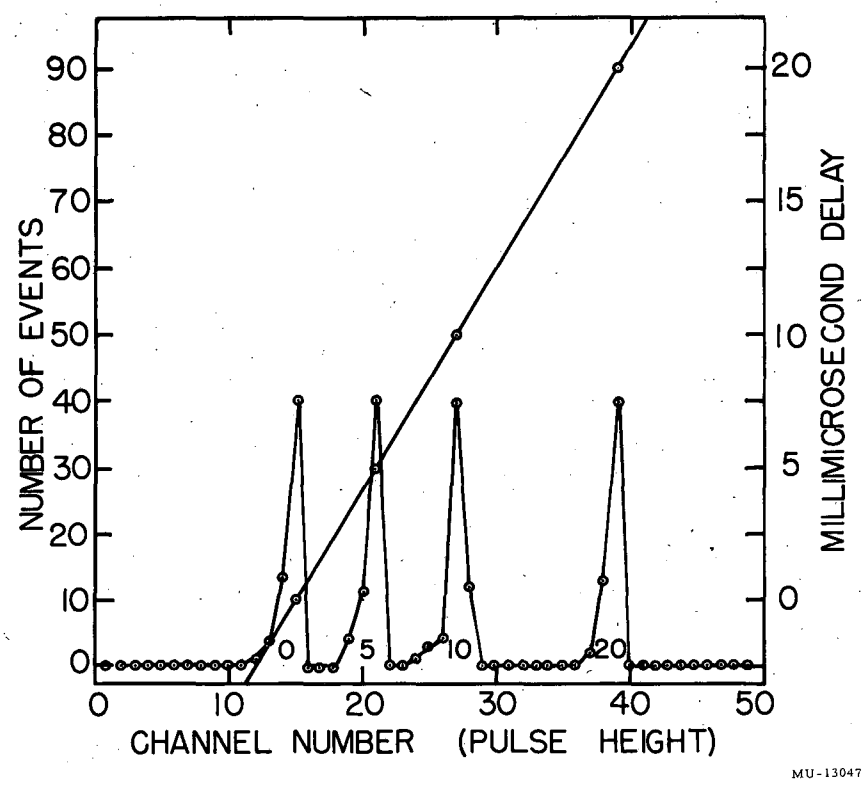

Fig. 13. Calibration curve of the time-to-height-converter (THC).

they would be limiting barriers to the improvement of the resolution.[23] So ordinarily peaks about eight channels wide at half-height are obtained corresponding to about 8×10^{-9} second. When 6BN6 electronic tubes having more than two grids are commercially made, triple coincidences can be used with the THC.

6. Electron-Electron Coincidences in Bi^{207}

An initial test on the coincidence circuit was made by feeding the K-conversion-electron pulses of the 1063.9-kev transition of Bi^{207} to the start pulse input of the THC, and the 569-kev transition to the stop pulse input. The lifetime of the 569-kev state from gamma-gamma coincidence measurements by Gerholm[24] is 0.9×10^{-10} sec. In other words, for this type of experiment the two transitions can be regarded as prompt and there should be no delay between the two events. The results are given in Fig. 14. The peak width at half-height (resolution) is 7.3×10^{-9} sec, corresponding to 8.75 channels. A delay between the two conversion electrons is evident from the shift of the peak position from channel 15 to channel 29.75, or a delay of 7.5×10^{-9} sec based on the peak centroid shift, which is impossible.

However, it must be remembered that the two electrons are traveling at different velocities. From fundamental laws the velocities are 0.97c and 0.48c for the 976-kev and 482-kev respectively, where c is the velocity of light. Since each has to travel a distance of 100 cm the difference in time between the two conversion electrons if they are emitted from the nucleus simultaneously amounts to 6.4×10^{-9} second. The difference between the central shift (delay), 7.5×10^{-9} sec and 6.4×10^{-9} sec, is within the experimental error. Therefore in all experiments with electrons of different energies, corrections due to difference in transit time should be applied.

In Fig. 14 a line L is drawn at the average value of the events per channel corresponding to the chance coincidence or the coincidence background per channel. In this result the chance coincidence was five counts per channel or 6 counts per millimicrosecond delay. If we add all the events that make up the peak and subtract the number of chance coincidences in that same area we obtain the true coincidence rate. In this case it amounts to:

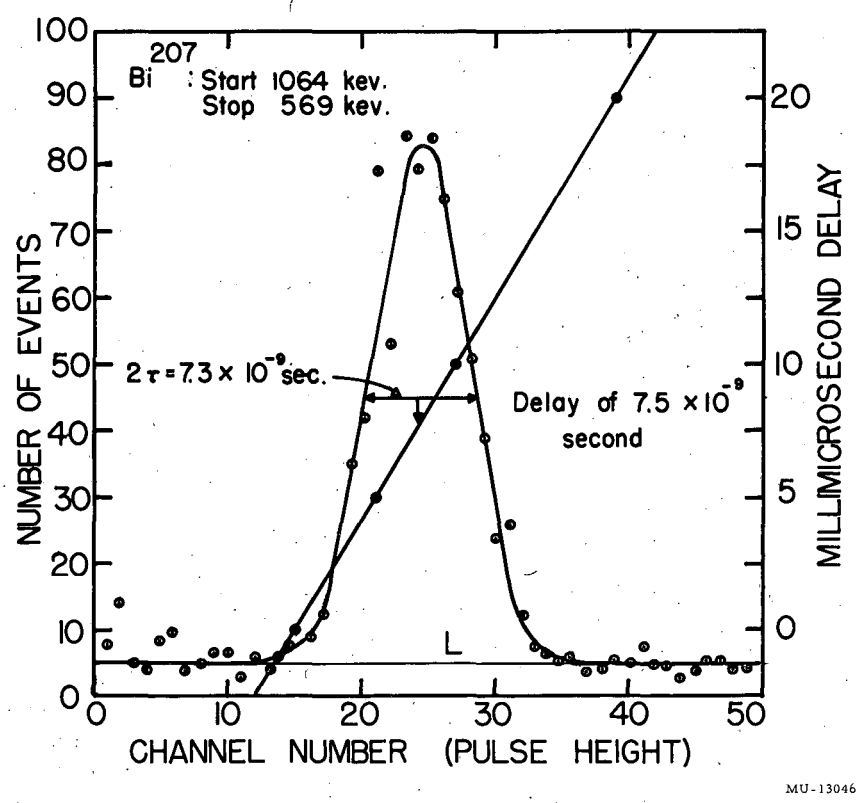

Fig. 14. THC coincidence spectrum for the 1064 kev ——→ 569-kev transition of Bi^{207}.

Sum of events from channel 14 to 38 inclusive (25 channels)	851
Total number of chance coincidences in 25 channels	125
True coincidences observed	726
True-to-chance ratio, 726/125	5.8

Immediately after obtaining the results with the 1064-kev → 569-kev transitions the stop side of the spectrometer current was increased to focus the conversion electrons of the 1064-kev transition. This should not be in coincidence, for both sides of the instrument are looking at the same transition. The results conclusively show they are not in coincidence, and are shown in Fig. 15.

7. Electron-Electron Coincidences in Hg^{203}

Similar electron-electron coincidence measurements were tried for Hg^{203}, whose 279-kev transition is in coincidence with the beta spectrum. By feeding the start pulses produced by the beta section of the spectrum and stopping with the pulses from either the K- or L-conversion electrons of the 279-kev transition, a peak was observed in the pulse-height analyzer. Since the energies of the beta particles and the conversion electrons were not too different from each other, the peak's centroid appeared at the zero delay channel. Previous investigators reported the lifetime of this state to be $< 2 \times 10^{-9}$ second.[25]

Hence, this electron-electron coincidence spectrometer would be a very powerful tool in the future solution and disentangling of the now complicated and unresolved decay schemes.

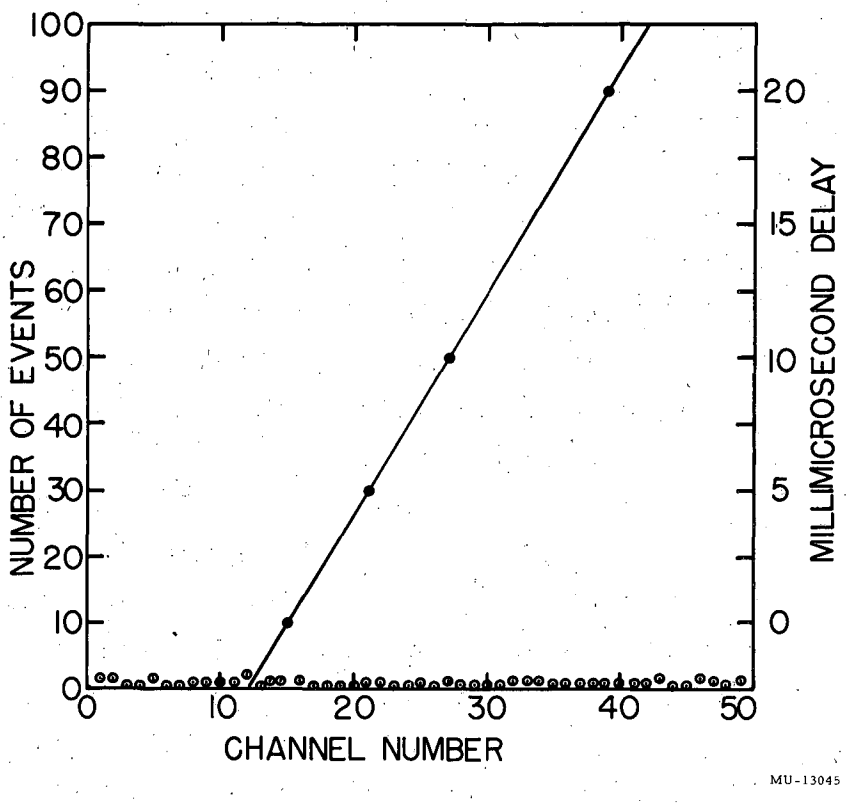

Fig. 15. THC coincidence spectrum of a typical noncoincident transition pair.

II. DECAY OF EUROPIUM-154

A. INTRODUCTION

Eu^{154} was first produced in 1938 by Scheichenberger,[26] using a neutron-capture reaction on natural europium. It decays principally by negatron emission, with a half-life given by Karraker et al.[27] of 16 ± 4 years. A number of studies[28-38] have been made of the gamma-ray and electron spectra of this isotope; however, the results are rather confusing. This is probably because Eu^{154} has been made together with 13-year Eu^{152} (natural europium is about an equal mixture of Eu^{151} and Eu^{153}), and due to the similarity of the decay schemes and half lives, it has been difficult to assign transitions with certainty to either isotope. As will be seen, this difficulty was not encountered in the present study.

From the studies made of Eu^{154}, the following information seems clearly established. A 123-kev gamma ray has been observed both from the decay of Eu^{154} [28,29] and from Coulomb excitation of Gd^{154}.[36] Andersson[34] measured the energy of this gamma ray to be 123.54 ± 0.09 kev, while Boehn and Hatch[30] reported this energy to be 123.07 kev. Sunyar observed that the level giving rise to this transition has a lifetime of 1.2×10^{-9} sec, which he used to classify the gamma ray as E2. The transition probabilities calculated from Coulomb excitation[36] and from Sunyar's[35] lifetime measurements agree within experimental accuracy. Huus et al.[36] measured the K/L ratio for this transition to be 1.0. Many higher-energy gamma rays and beta end points have been reported, but, as has been mentioned, the agreement among these data has been poor. Recently, Kedzie et al.[37] have determined the spin of Eu^{154} to be 3 and the magnetic moment to be 2 n.m. by observing the microwave paramagnetic resonance hyperfine structure. Also, gamma-gamma coincidences were made by Stephens,[38] whose results are in agreement with this investigation.

The europium used in this study was furnished by T. Parsons, S. G. Thompson, and R. Silva; it was prepared by irradiating plutonium for about two years in the Materials Testing Reactor at Arco, Idaho. In this manner, Eu^{154} was produced from neutron capture on fission

products, and hence no Eu^{152} was present in the sample. In order to separate europium from the plutonium and from the many fission products, the following chemical procedure was used. The sample, contained in an aluminum ring, was dissolved in a $NaOH-NaNO_3$ solution. This procedure left the actinides and lanthanides (and many other fission products) as precipitates, but dissolved the aluminum ring. The precipitate was then dissolved in hydrochloric acid solution and the actinides and lanthanides reprecipitated as fluorides, separating them from most of the other fission products. The fluoride precipitate was dissolved in boric acid and the lanthanides and actinides reprecipitated with the addition of hydroxide. This precipitate was treated with hydrochloric acid solution and evaporated almost to dryness. A 10.5 M solution of LiCl was used to dissolve the residue and the solution was passed through a column of Dowex A-1 anion resin maintained at 80°C. The lanthanides came through this column almost immediately, whereas the actinides were held up for some time. The lithium was removed from the lanthanides by precipitating the latter as hydroxides and then redissolving the precipitate in hydrochloric acid. To separate the europium from the other lanthanide elements, the material was placed on a column containing Dowex-50 cation resin and maintained at 80°C. The lanthanides were then eluted in an ammonium alpha-hydroxyisobutyrate solution, which brought them off the column individually, in order of decreasing atomic number. To insure complete separation the europium fraction was passed through a second "isobutyrate column." From the purified europium solution samples were prepared for analysis of the electron spectrum by electrodeposition onto a 0.010-in.-diameter platinum wire. The samples for the gamma-ray studies were evaporated on 0.006-in.-thick aluminum plates.

Europium samples from two separate plutonium irradiations were used in this work. Both samples give the same results with the exception that the low-energy gamma rays of Eu^{155} were found to be less intense in the first sample, which had been out of the reactor for 3 to 4 years. This is sufficient time for an appreciable decay of 2-year Eu^{155} to occur. The second sample was mass-analyzed and the following constituents reported: Eu^{155}, 6.5%; Eu^{154}, 15.2%; Eu^{153},

78.9%, Eu^{152}, $<0.1\%$. The Eu^{152} was below the limit of detection of the mass analysis, and there was no evidence for its presence in the gamma-ray or electron data.

B. EXPERIMENTAL

1. Conversion-Electron Results

The conversion-electron and beta-ray spectrum of Eu^{154} was studied on two types of instruments. The first type included the four 180° permanent-magnet electron spectrographs described previously by Smith and Hollander.[39] These instruments were used principally to measure the conversion-electron energies with high precision. The conversion-electron lines were recorded photographically on glass-backed Eastman No-Screen x-ray plates having an emulsion thickness of 25 microns. The resolution (full width of a peak at one-half its maximum) of these spectrographs in the present experiments was about 0.1%. In order to obtain the best possible energies, the 123.07-kev transition measured by Boehn and Hatch[30] was used as an internal energy standard.

Measurements of the electron spectrum of Eu^{154} were also made using a double-focusing semicircular magnetic beta-ray spectrometer having a radius of 25 cm.[11,40] The focused electrons were detected with a thin-window Geiger counter in this instrument with a resolution of about 0.5%. The relative intensities of the conversion electrons were determined considerably more accurately with this instrument than on the permanent magnets, and it was also possible to investigate the high-energy beta end points.

The conversion-electron data taken on these instruments are summarized in Table II. The energy measurements are from the permanent-magnet spectrographs, and the limit of error on these energies is expected to be 0.1%. The qualitative relative-intensity data from the permanent magnets are given in columns 2 and 3, whereas the numerical values from the double-focusing spectrometer are listed in column 4. The errors associated with the relative-intensity data taken on the double-focusing spectrometer are estimated to be about 20%. The assignment of the lines in Table II is straightforward, and,

TABLE II

Conversion Electron Lines of Eu^{154}

Electron Energy	P.M. Intensity*	D.F. Intensity	Conv. Shell	E_γ	Transition Energy**
72.67	vvvs	100	K	122.9	
114.52	vs		L_I	122.9	
115.10	vvs	109	L_{II}	123.0	
115.65	vvs		L_{III}	122.9	(123.07)***
121.1	ms	18.9	M	123.0	
122.6	wm	---	N	123.0	
197.7	wm	3.1	K	247.9	(248.08)***
239.6	--	1.2	L_I	248.0	
543.1	ms	--	K	593.3	593.3
643.6	vvw	0.55	K	694.1	694.1
685.6	vw	--	L_I	694.0	
655.6	vvw	--	K	705.8	705.8
697.4	vvw	--	L_I	705.8	
703.8	vvw	--	M	705.7	
674.7	vs	0.31	K	724.9	724.9
716.4	vvw	--	L_I	724.8	
722.6	vvw	--	M	724.5	
708.7	m	0.08	K	758.9	758.9
825.1	ms	0.40	K	875.3	875.3
867.0	--	--	L_I	875.4	
948.0	ms	0.15	K	998.2	998.2
990.2	--	--	L_I	998.6	
956.7	s	0.39	K	1006.9	1006.9
998.8	--	--	L_I	1007.2	
1226.5	w	0.37	K	1276.7	1276.7
1268.4	vvw	--	L_I	1276.8	

* v = very, s = strong, m = moderate, w = weak.

** Errors estimated to be ± 0.1%.

*** From Boehm and Hatch's bent-crystal measurements.[30]

as will be seen, is in good agreement with the gamma-ray and coincidence data (Table III).

In addition to the electron lines, it was possible to determine beta end points at 1850, 875, 596, and 250 kev. At lower energies quite a unique resolution (allowed) of the Fermi-Kurie plot could not be obtained. The reason for this is not clear; however, it might be at least partially explained if the above data groups had forbidden rather than allowed shapes. It will be shown that the log ft values for these transitions are all 10 or larger. Because of these uncertainties and others which will be discussed later, it was not possible to obtain reliable relative intensities for any of the beta groups.

2. Gamma-Ray Spectrum and Gamma-Gamma Coincidence

(This part was done in cooperation with F. S. Stephens, Jr.)

To study the gamma-ray spectrum of Eu^{154}, a NaI(Tl) crystal coupled to a 50-channel pulse-height analyzer was used. A resolution (full width of a peak at half maximum divided by the energy of the peak) of about 8% was obtained for the 661-kev gamma ray of Cs^{137}. For coincidence work the 50-channel analyzer could be gated with the output of a single-channel analyzer, which analyzed the spectrum of a second NaI(Tl) crystal. A resolving time (2τ) of about two microseconds was used in these experiments. This equipment has been described in detail elsewhere.[38] Counting efficiency and escape peak corrections for the NaI crystal have been applied to all the gamma-ray intensities considered.

A portion of the gamma-ray spectrum of Eu^{154} is shown in Fig. 16a. The resolution of this region into five gamma rays is also indicated, and was made using the peak shapes measured for the following single photopeaks: Cs^{137}, 0.661; Mn^{54}, 0.84; Bi^{207}, 1.063; Na^{22}, 1.277 Mev. The resolution of the gamma ray at 0.60 Mev is not very reliable, and its relative intensity is particularly uncertain due to the low abundance of this peak and the large amount of Compton radiation beneath it. There is a slight indication of a peak around 1.1 Mev; however, its intensity both in the gamma-ray spectrum and in the coincidence work was too low for careful study. Other gamma rays

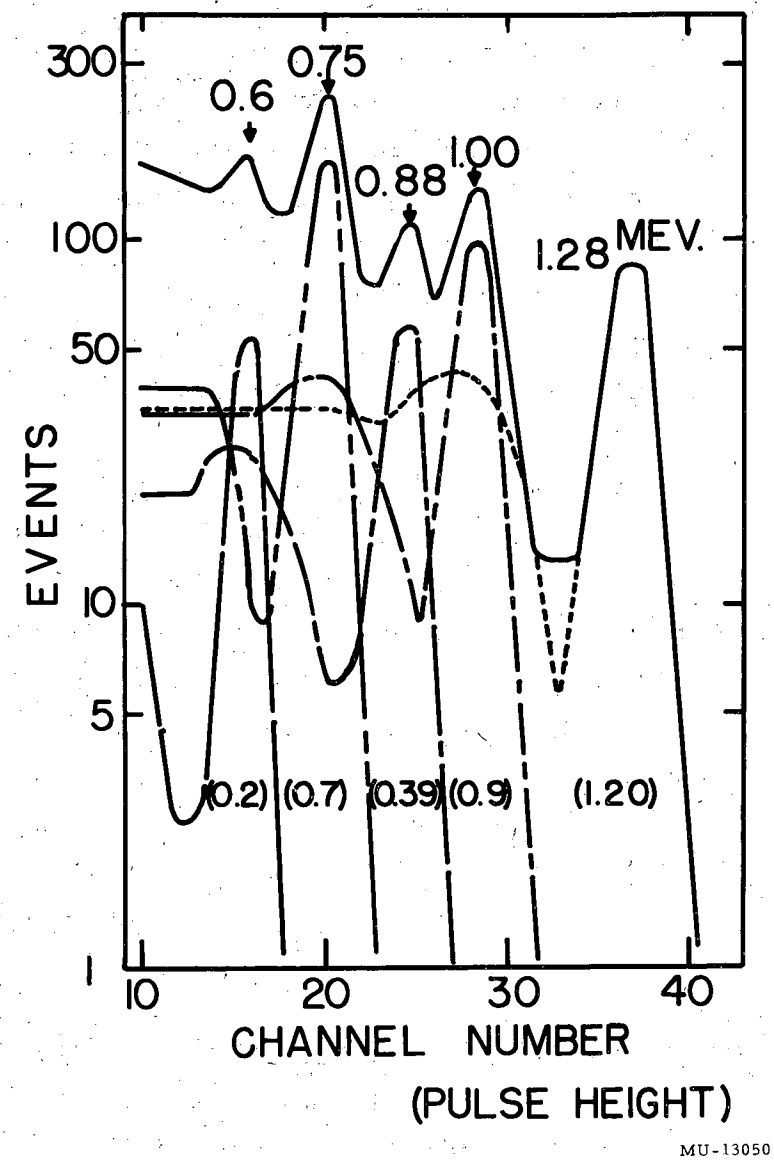

Fig. 16a. Portion of gamma-ray spectrum of Eu^{154}, showing resolution into five gamma rays, and their relative intensities.

in the sample at 0.12, 0.25, and ~1.6 Mev were observed and assigned to Eu^{154}. The low-energy gamma rays of Eu^{155} were also present. Table III lists the best energies and relative intensities of the Eu^{154} gamma rays. An intensity of the 0.25-Mev gamma ray was not obtained due to the fact that a backscattering peak from the higher-energy gamma ray is expected at about this energy, and it was not certain how much of this peak was caused by true nuclear 0.25-Mev photons. The peak at ~1.6 Mev was not a single peak, and the intensity listed is a maximum intensity for radiation higher in energy than 1.28 Mev. The relative intensities listed are the average of four determinations, and from the reproducibility of these results it is estimated that they should be good to 10 to 15%.

The gamma-ray spectrum in coincidence with the 0.12-Mev photons is shown in Fig. 16b. Its resolution is also indicated and the relative abundance of the peaks is given in Table III. The intensity of the 1.28-Mev peak has been normalized to the value of the gamma-ray spectrum. The intensities listed are the averages of two determinations, and again are expected to be good to 10 to 15%. It should be added that in these measurements the coincidence rate due to the Compton-scattered radiation beneath the 0.12-Mev peak was determined by setting the gate just above this peak and running for an equal length of time. This small contribution was then subtracted from the total coincidence curve.

TABLE III

Gamma-Ray and Coincidence Abundances

E_γ Mev	γ ray Rel. Abund.	Coincidence with 0.123 Rel. Abund.	Coincidence with 0.73 Rel. Abund.	Coincidence with 1.0 Abs. Abund.	Coincidence with 1.28 Abs. Abund.
0.040	--*	--	--	--	0.20
0.123	(1.00)	--	--	--	0.40
0.60	0.2	0.1	--	0.12***	x
0.75	0.70	0.29	--	0.34	x
0.88	0.39	0.35	(0.37)	x	x
1.00	0.90	0.50	0.39	x	x
1.28	1.20	(1.20)	x**	x	x
~1.6	0	--	--	--	--

* Indicated either no data or an ambiguous result.
** x indicates no coincidence.
*** Absolute abundances given in photons per "gate" photon.

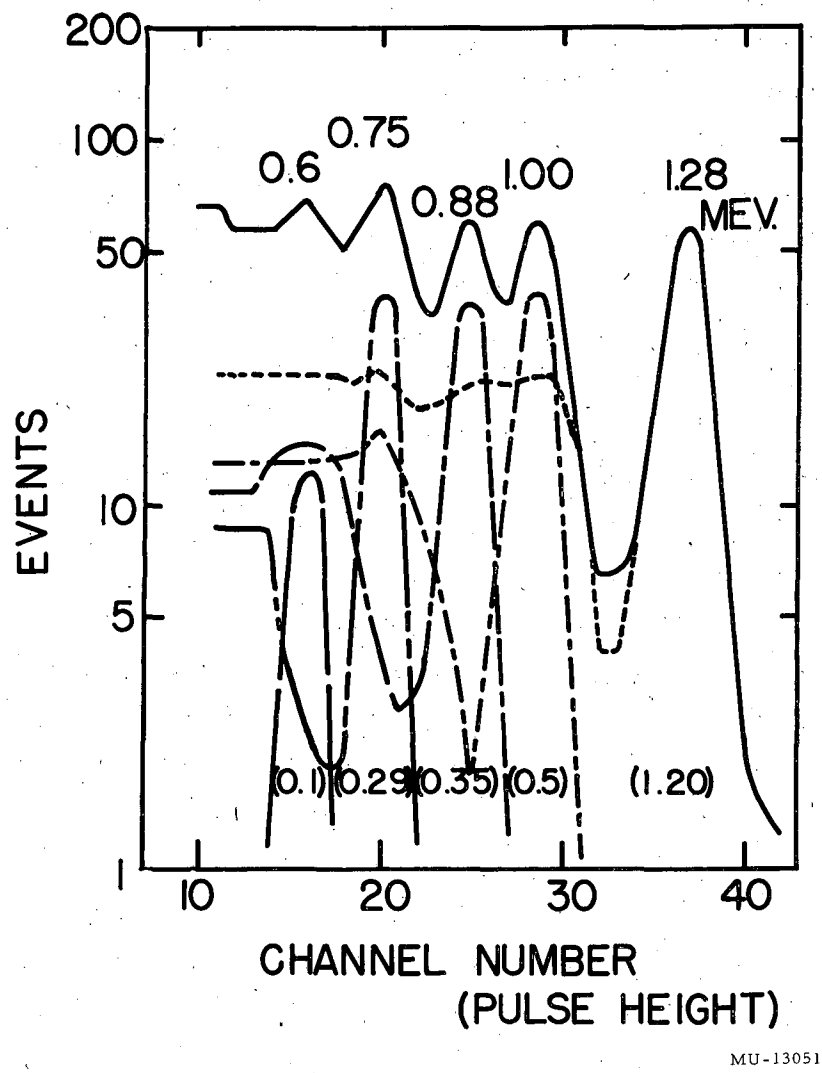

Fig. 16b. Gamma-ray spectrum of Eu^{154} in coincidence with 0.12-Mev photons, showing resolution into five gamma rays, and their relative intensities.

Coincidences among the higher-energy gamma rays were complicated by the fact that beneath each photopeak (except the one at 1.28 Mev) there is a large contribution from the Compton distributions of higher energy. For this reason, some of the relative intensities measured were not meaningful, and in a few cases ambiguities arose as to whether a coincidence did or did not exist. The results of some of these measurements have been included in Table III. Inconclusive measurements have been indicated by a dash (-), whereas a cross (x) indicates that there was definitely not a coincidence. Only relative intensities were obtained from the spectrum in coincidence with the 0.73-Mev gamma ray, and in this case the intensity of the 0.88-Mev peak was normalized to the average intensity of this peak from the preceding two columns.

From the knowledge of the "gate" counting rate and the solid angle subtended by the "signal" NaI crystal, it was possible to obtain absolute intensities for the radiations in coincidence with the 1.0- and 1.28-Mev gamma rays. In the case of the 1.28-Mev gate, a subsequent run was made with the gating energy just above the 1.28-Mev peak, and both the coincidences and the "gates" from this run were subtracted from those of the true 1.28-Mev coincidence measurement. The resulting spectrum is shown in Fig. 17, and it is seen that only the 0.12-Mev gamma ray and a peak at 0.04 Mev are present. The latter peak is almost undoubtedly gadolinium K x-rays. The intensity of these two peaks per 1.28-Mev gate is given in Table III. In order to obtain absolute intensities of the gamma rays in coincidence with the 1.0-Mev photons, it was necessary to subtract from the gate counting rate those counts that were due to Compton-scattered radiation from the 1.28-Mev gamma ray. This was accomplished by assuming the same ratio of Compton-scattered radiation at 1.0 Mev to photopeak height at 1.28 Mev for Eu^{154} as was measured using a Na^{22} source. Both sources were on 0.006-in. aluminum plates and the geometrical conditions were as nearly identical as possible. Since the 1.28-Mev gamma ray of Eu^{154} was found not to be in coincidence with any radiation above 0.12 Mev, it was safe to assume that the Compton radiation beneath the 1.0-Mev peak did not contribute to the high-energy coincidence counting rate.

Beta-gamma coincidences were measured also using an anthracene crystal as the electron detector; however, due to the many beta components

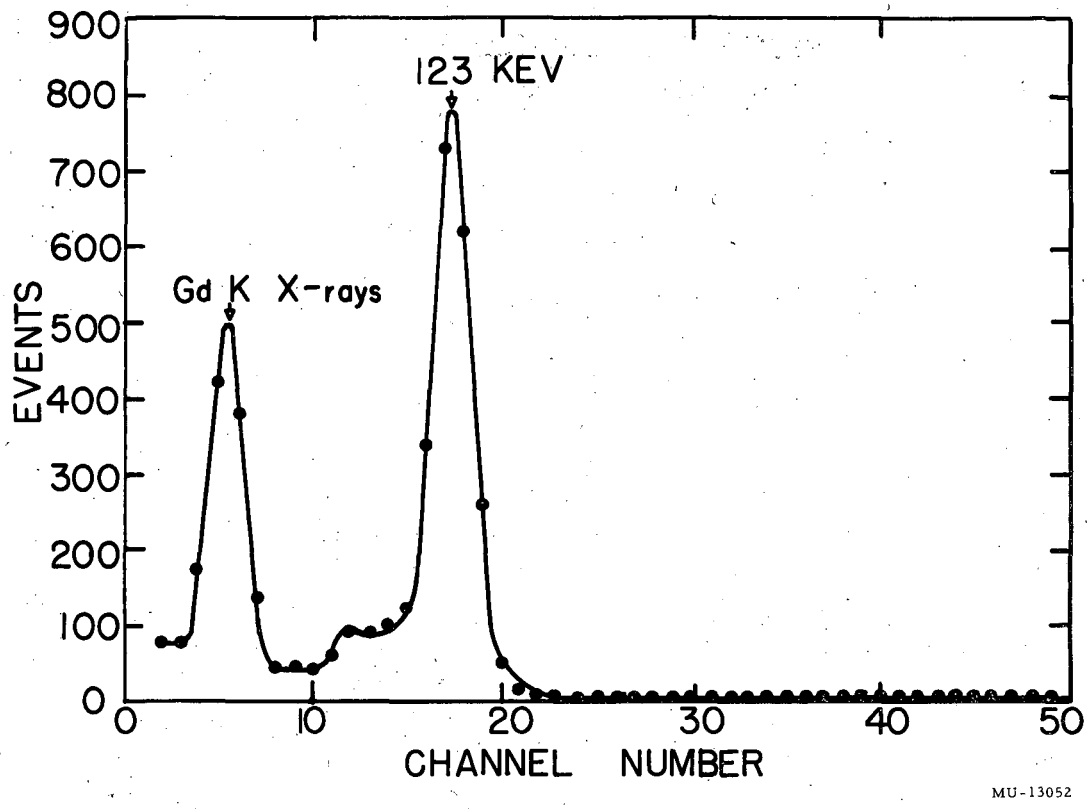

Fig. 17. Gamma ray spectrum of Eu^{154} in coincidence with 128-Mev photons.

present, these measurements were not very helpful. It was possible to show, however, that the very highest-energy beta particles were in coincidence with the 0.12-Mev gamma ray in an intensity of about 0.4 per beta particle.

3. Electron-Electron Coincidences

Coincidence measurements using the electron-electron coincidence spectrometer were also performed (see Part I). With the 123.0-kev transition as the stop signal, the beta-spectrum pulses were fed into the start pulse input. Enough events were collected for each case, and runs were made as long as two days where the counting rate was small. Since the results were collected in the form of a pulse-height distribution these were analyzed in the same way as Bi^{207} and Hg^{203}. When the original beta spectrum was normalized to the beta spectrum in coincidence with the 123.0-kev transition by dividing it with an arbitrary constant, the fit was within experimental accuracy except near the 250-kev region and lower, where the beta-spectrum contribution of Eu^{155} was responsible for the higher counting rate of the original beta spectrum. The results are shown in Fig. 18, and it shows that the highest-energy beta component is in coincidence with the 123.0-kev transition, in agreement with the proposed decay scheme in Fig. 19.

There were only two transitions in Eu^{154} whose conversion electrons were strong enough to be feasible for electron-electron measurements. These are the 123.0- and 247.9-kev transitions. The results of the measurements are:

TABLE IV

Start pulse	Stop pulse	Time (min)	Chance Coincidence	True Coincidence	True / Chance coincidence
K of 123 kev + β^-	K of 123 kev + β^-	400	150	493	3.3
K of 247 kev + β^-	K of 123 kev + β^-	1194	140	1273	9.1

Since the same stop pulses were used in both cases the only differences in the two measurements are the start pulses. The 123.0-kev plus beta-continuum pulses are much more intense than the 247.9-kev plus beta pulses; hence the reason for their higher counting rate, both for true

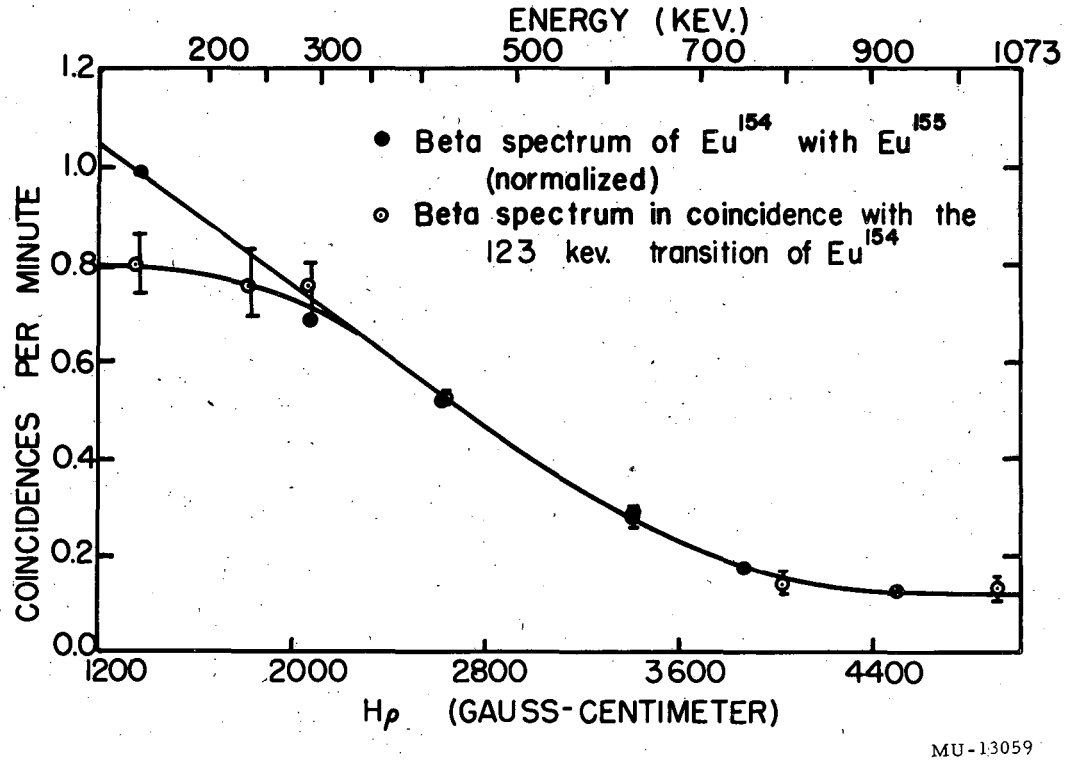

Fig. 18. Part of the beta-ray spectrum of Eu^{154} in coincidence with 0.12-Mev K-conversion electrons (normalized).

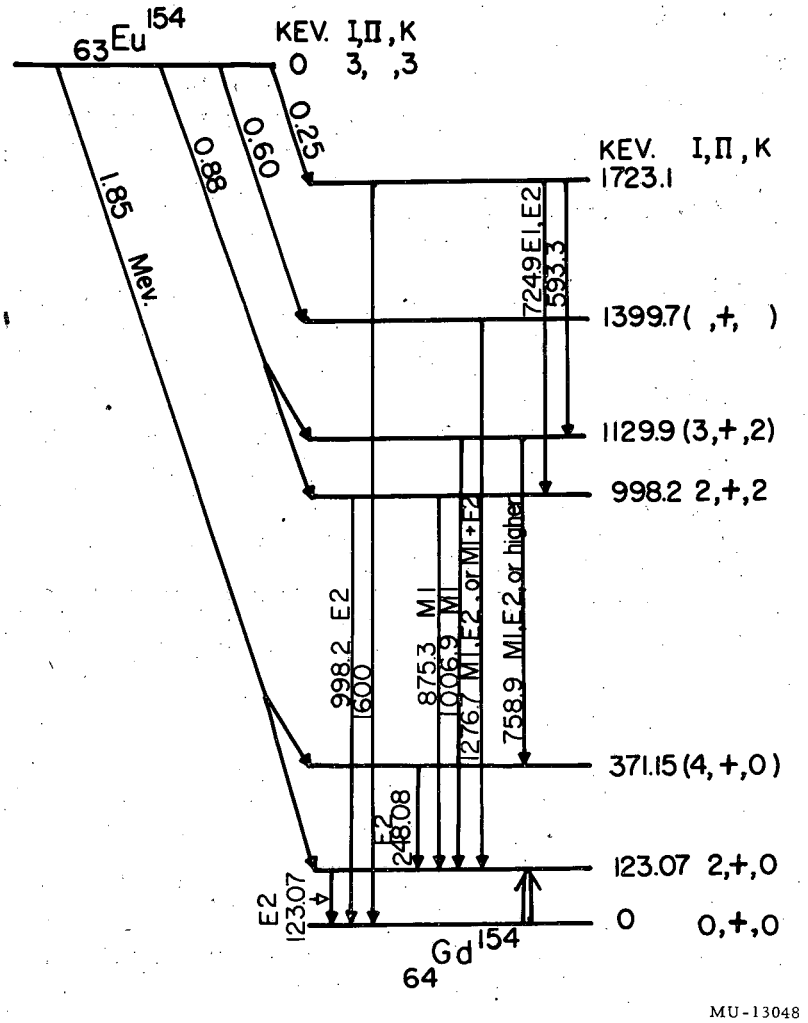

Fig. 19. Decay scheme of Eu^{154}.

and chance coincidences. However, the true-to-chance coincidence ratio increased by 2.8 times in spite of the fewer events detected per unit time in the second case, showing that the conversion electrons of the 247.9-kev riding on top of the beta spectrum is in coincidence with the 123.0-kev transition, again agreeing with the proposed decay scheme shown in Fig. 19 and with the gamma-gamma coincidence results.

4. Decay Scheme

The level scheme of Gd^{154} is readily deduced from the precise gamma-ray energies calculated from the conversion-electron energies and the gamma-ray coincidence data. It is shown in Fig. 19. The energy sums all agree to within 0.1%. The gamma-ray and coincidence data will presently be shown to be in good agreement quantitatively with this decay scheme. Only two gamma transitions seen on the permanent magnets have not been placed in Fig. 19. These are the 0.694_1- and the 0.705_8-Mev gamma rays. It is interesting that their sum is 1.399_9 Mev, which is well within the limit of error of the 1.400-Mev level; however, there is not considered to be sufficient evidence to place them in the decay scheme at present. It will be seen that there is no evidence that an appreciable number of 0.694 photons are present in the gamma-ray spectrum, which, considering the large electron intensity in Table II, is somewhat surprising. This leads one to believe that the 694-kev transition is highly converted.

Cork et al.[41] reported two intense transitions which were not seen previously; these were 84.2 and 344.3 kev. However, no such transitions were found in this study in spite of the efforts made to see them. The explanation may be that they belong to Eu^{152}, whose first excited state is 344 kev in the gadolinium side of the decay, or they could belong to an isomer of Eu^{154} if this could be identified. Toth[42] in his preliminary gamma-spectrum results of Tb^{154}, which decays by E.C. to Gd^{154}, observed also a 350-kev gamma ray present half as intense as the 247-kev photon. It seems that the 123- and 247-kev photopeaks decay with a different half-life compared to that of the 350-kev photopeak. Whether this 350-kev belongs to Gd^{154} or not can be determined by gamma-gamma coincidences of the 344-kev with the 123- and 247-kev photopeaks in Tb^{154}. However, the absence of the 344.8- and 84.2-kev transitions agrees well with the experimental transition-intensity results for Eu^{154}.

It is possible to calculate a K-conversion coefficient (α_k) for the 0.12-Mev transition from the spectrum in coincidence with the 1.28-Mev gamma ray, which is shown in Fig. 17. If a K fluorescence yield of 0.93 is used for gadolinium[43] and if all the K x-rays in Fig. 17 are assumed to arise from the conversion electrons of the 0.12-Mev transition, then α_K may be calculated to be 0,54. Also, since one would expect each 1.28-Mev gamma ray to be followed by one 0.12-Mev transition, a total conversion coefficient (α_t) of 1.5 can be deduced for the 0.12-Mev gamma ray. Hence, from the scintillation counter data alone the ratio α_K/α_t is determined to be 0.36. An independent value for this ratio may be calculated from the electron data of Table II, if N-shell and higher-level conversions are assumed to be negligible. To within a very few percent, this assumption is almost undoubtedly correct, and leads to a ratio, α_K/α_t, of 0.44 from the electron data. The agreement between the two methods is seen to be quite reasonably good. Since a K/L ratio of 0.9 is readily calculated from the electron intensities, an absolute L-conversion coefficient of 0.60 is obtained by combining the electron and gamma-ray data. Theoretical estimates of the K (Sliv[44]) and L (Rose[45]) conversion coefficients for this energy and the atomic numbers for E1, E2, and M1 transitions are given in Table V.

TABLE V

Conversion Coefficient of the 0.123-Mev Transition

	E1	E2	M1	Experimental
K	0.14	0.65	1.1	0.54
L	0.02	0.5	0.2	0.60
Total	0.17	1.5	1.4	1.5

The transition is clearly E2, in agreement with Sunyar's[35] conclusion from the lifetime, and with the qualitative L-subshell ratio from the permanent-magnet spectrograph. It is worth mentioning that the experimental α_K is lower than Sliv's theoretical value by about 10%.

A comparison of the scintillation-counter intensities (Table III) with the decay scheme of Fig. 19 is now in order. It can be seen from the decay scheme that, of the gamma rays resolved in Fig. 16a, three are

expected to decay essentially completely through the 0.12-Mev level. These are at energies of 1.28, 0.88, and 0.60 Mev. Since the intensity of the 1.28-Mev gamma ray is the most precisely measured of these three, it was used to normalize the gamma-ray and coincidence relative-intensity data shown in Table III. When this was done, it was noted that the two intensities measured for the 0.88-Mev gamma ray agreed to within about 10%. Because the intensities of the 0.60 transition are considerably less accurately known, they are not considered to be in disagreement with each other. The data, then, are consistent with each of these three gamma rays being completely in coincidence with the 0.12-Mev transition. We next consider the 1.0-Mev peak. The electron spectrum shows two gamma rays, and this peak is expected to include the 1.007- and the 0.998-Mev gamma rays. Of these, the 1.007-Mev gamma ray is expected to be in coincidence with the 0.12-Mev transition, while the 0.998-Mev gamma ray is not. Thus, the 0.50 measured as the relative intensity of the 1.0-Mev peak in the spectrum coincidence with 0.12-Mev photons must be due to the 1.007-Mev gamma ray; and the residual intensity of 0.40 should be attributed to the 0.998-Mev gamma ray. This may be checked by considering the spectrum in coincidence with the 0.73-Mev photons. This spectrum should include the 0.88- and 0.998-Mev gamma rays in their true relative intensity, and should include no 1.007-Mev photons. Accordingly, the intensity of the 0.88-Mev gamma ray in this spectrum (col. 3, Table III) was normalized to the average intensity of this transition in the other two measurements, and an intensity of 0.39 was obtained for the 0.998-Mev gamma ray. This is in good agreement with the value of 0.40 arrived at independently above. Considering now the 0.73-Mev transition, we note that of the coincidences with the 1.0-Mev peak, only the 0.998-Mev photons are preceded by a 0.725-Mev gamma ray, while only the 1.007-Mev photons are preceded by a 0.60-Mev gamma ray. Since the relative intensities of the two components of the 1.0-Mev peak are now known, the absolute intensity data in Table III may be corrected to the following: 78% of the 0.73-Mev photons per 0.998-Mev gate; and 21% of the 0.60-Mev photons per 1.007-Mev gate. The total intensity of the 0.725-Mev gamma ray is then expected to be 78% of the combined intensity of the 0.88- and 0.998-Mev transitions, or,

relative to the numbers in Table III, 0.60. An independent maximum intensity for the 0.725-Mev transition may be obtained from the intensity of the 0.73-Mev peak in coincidence with the 0.12-Mev photons. This peak will contain at least the 0.725- and the 0.759-Mev gamma ray, but by considering the 0.759-Mev intensity to be negligible, we may calculate a maximum intensity for the 0.725-Mev gamma ray. It is necessary to increase the relative intensity of 0.29 from Table III by the ratio of total radiation from the 0.998-Mev level to 0.88-Mev radiation, since only the fraction of the 0.73-Mev photons which are followed by the 0.88-Mev gamma rays is subsequently followed by a 0.12-Mev transition. This ratio has been determined to be 2.1, giving a total maximum intensity of the 0.725-Mev gamma ray of 0.60. A second upper limit on the intensity of the 0.73-Mev gamma ray is the total intensity of radiation in this energy region observed in the gamma-ray spectrum. From Table III, this upper limit is 0.70. Thus, a measured value and two upper limits on the intensity of the 0.725-Mev gamma ray has been determined to be 0.60, 0.60, and 0.70 respectively. Within the limits of error of the measurements, these numbers probably do not differ. This is taken to indicate that the gamma rays of 0.705, 0.694, and 0.759 Mev are all weak compared to the 0.725-Mev transition, whose abundance relative to the numbers in Table III is about 0.6. In addition to the two values for the relative intensity of the 0.60-Mev gamma ray listed in Table III, a third and probably more accurate value may be calculated by using the result that the 1.007-Mev transition is preceded by a 0.60-Mev photon 21% of the time. Considering that the 0.758-Mev transition is of negligible intensity compared to the one at 1.007 Mev, an abundance of 0.11 is obtained for the 0.60-Mev transition. This is in reasonable agreement with the 0.1 and 0.2 listed in Table III for this transition.

The relative intensities in Table III and those derived in the preceding discussion may be converted into absolute intensities in the following manner. The beta-gamma coincidence measurements showed that the very highest-energy beta particles were in coincidence with about 0.4 of the 0.12-Mev photons. Using the conversion coefficient of 1.5 determined for the 0.12-Mev transition, this result indicates that even the highest-energy beta particles measured are in coincidence with the

0.12-Mev transition. Direct beta population of the ground state is thus shown to be small compared with population to the 0.12-Mev level, which itself will presently be shown to be only around 5%. From the decay scheme in Fig. 19 it is seen that only two gamma transitions terminate at the ground state. These are at energies of 0.999 and 0.12 Mev, and together must carry all the beta decay, since there is no appreciable direct beta population of the ground state. Using the sum of these transition intensities to determine the beta-decay rate, the absolute gamma-ray intensities listed in Table III were calculated. The limit on the 0.694; 0.705; and 0.756-Mev gamma rays was obtained by concluding from the discussion of the preceding paragraph that none of these is over 15% as large as the 0.725-Mev gamma ray. From the measured K-conversion coefficient of 0.54 for the 0.12-Mev transition, the absolute electron intensities can also be calculated, and these are listed in column 3 of Table III. The resulting K-conversion coefficients together with the theoretical values of Sliv and the probable multipolarity of the gamma rays are included in Table VI. The limits of error on the conversion coefficients are expected to be about 20 to 30%. Since a 50% error would be sufficient to change the multipolarity assignment in many cases, the assignments made in Table VI should be considered somewhat tentative. However, for the most part the agreement with the theoretical value is good, and there is no evidence to indicate that any assignment is incorrect.

From gamma-ray and conversion-electron intensities no multipolarity can be assigned to the 248-kev transition. So, the K/L conversion electron relative intensity was used. An experimental value of 2.6 ± 0.6 was found, and this agrees quite well for an E2 transition. The theoretical and observed K/L ratios are:

	M1	M2	E1	E2	Experimental
K/L	7	5	6	3	2.6 ± 0.6

From the gamma-ray intensities in Table VI and the decay scheme shown in Fig. 19, it is possible to reconstruct the beta spectrum. The population to the 1.724-Mev level is simply the sum of the intensities of the 0.60; 0.725; and 1.6-Mev gamma rays, or about 28%. Similarly the

TABLE VI

Gamma-Ray and Conversion-Electron Absolute Abundances of Eu^{154}, and Multipolarity Assignment

E_γ	γ ray Abs.Abun.	K Electron Abs.Abun.	α_k Exp.	α_k* El	α_k E2	α_k M1	α_k M2	Probable Multipolarity
0.123	0.35	(0.19)	(0.54)	See Table III				E2
0.248	--	0.0059	--	--	--	--	--	E2**
0.593	0.04	--	--	--	--	--	--	--
0.694	<0.035	1.0×10^{-3}	$>2.9\times10^{-2}$					M2 or higher
0.706	<0.035	--	--	1.9×10^{-3}	4.9×10^{-3}	9.0×10^{-3}	2.4×10^{-2}	--
0.725	0.21	5.9×10^{-4}	2.8×10^{-3}					E1,E2
0.759	<0.035	1.6×10^{-4}	$>5.0\times10^{-3}$					M1,E2, or higher
0.875	0.13	7.6×10^{-4}	5.8×10^{-3}	1.4×10^{-3}	3.3×10^{-3}	5.8×10^{-3}	1.5×10^{-2}	M1
0.999	0.14	2.9×10^{-4}	2.1×10^{-3}	1.1×10^{-3}	2.4×10^{-3}	4.2×10^{-3}	1.0×10^{-2}	E2
1.007	0.17	7.4×10^{-4}	4.4×10^{-3}					M1
1.277	0.42	7.0×10^{-4}	1.7×10^{-3}	7.0×10^{-4}	1.5×10^{-3}	2.4×10^{-3}	5.7×10^{-3}	M1,E2,M1-E2
~1.6	0.0	--	--	--	--	--	--	--

* Theoretical K-conversion coefficients of Sliv.

** From K/L conversion-electron ratio.

population to the 1.400-Mev level is just equal to the intensity of the 1.277-Mev transition, or 42%. For the 1.130- and 0.998-Mev levels, it is necessary to sum the intensities of the gamma rays de-exciting each of these levels and subtract from this the intensity of the photons populating the level. The difference must be accounted for as direct beta population, and turns out to be 13 and 6% respectively for these levels. In this calculation the 0.759-Mev gamma ray has not been included, since its measured intensity is only an upper limit. It should be pointed out that the low-intensity beta groups, both those mentioned above and those which will be mentioned below, result from differences between rather large gamma-ray intensities, and hence have large limits of error associated with them. If the intensities of all the gamma rays populating any of the three lowest levels are summed, a total of about 88% of the beta transitions is accounted for. This implies that a total of around 12% of the beta population goes directly to the three lowest levels. It has already been shown that the ground state receives essentially no direct population, so that the 12% must be divided between the 0.123- and 0.371-Mev levels. There are not sufficient data to determine unambiguously how this 12% is distributed; however, the following argument may be made. The 0.248-Mev gamma ray is very likely electric quadrupole, in agreement with the rotational model of Bohr and Mottelson.[46] If this is so, one may calculate from the intensity of the K electrons of this transition and the theoretical K-conversion coefficients of Sliv[44] that the gamma ray should have an abundance of 8 or 9%. Somewhere between 1 and 3% of this probably comes from gamma-ray rather than direct beta population of the 0.371-Mev level. This leaves 5 to 8% for direct beta population, which in turn leaves 4 to 7% for direct population to the 0.123-Mev level. The highest-energy portion of the beta spectrum was re-examined to see if the Fermi-Kurie plot was consistent with the above conclusions, and it was found that the population to the 0.371-Mev level could be anywhere from zero to about equal to the amount going to the 0.123-Mev level. Thus, there is no inconsistency with the highest-energy beta groups populating the 0.123- and 0.371-Mev levels about equally. Table VII summarizes the beta groups and lists the log ft value for each group. The total beta-decay energy of

1.97 Mev was obtained from the highest-energy beta end point of 1.85 Mev together with the coincident 0.12-Mev gamma ray.

TABLE VII

Beta Groups of Eu^{154} (Indirect)

Energy (Mev)	Abundance %	log ft
0.25	28 ± 5	9.0
0.59	42 ± 5	10.0
0.86	13 ± 5	11.0
0.99	6 ± 5	11.6
1.63	6 ± 5	12.5
1.85	6 ± 5	12.9

The spin and parity assignments shown in Fig. 19 are all rather easily deduced. The parity of all the states except the one at 1.724 Mev must be even (+), since the transitions are all either M1 or E2. Since it was not possible to decide between E1 and E2 for the 0.725-Mev gamma ray, the 1.724-Mev level could have either even or odd parity. The spin of the 0.123-Mev level is certainly two, since the 0.123-Mev transition has been shown to be E2. The spin and parity of the 0.371-Mev level are only tentative, but are assigned on the basis of the Bohr-Mottelson theory and the absence of the cross-over transition to the ground state. The E2 character of the 0.998-Mev gamma ray fixes the spin of the 0.998-Mev level at two. The suggested spin of the 1.130-Mev level will be considered in the following section.

C. DISCUSSIONS

Gd^{154}, with 90 neutrons, lies just within the region of the rare earth nuclides, where the Bohr-Mottelson[46] collective nuclear model is applicable. It has been shown that a rather sudden change from the transition region into the strong-coupling region occurs between neutron numbers 88 and 90. This shift is readily observed in the first excited-state energies of Gd^{152} and Gd^{154}, which are 344 and 123 kev respectively. Since Gd^{154} is at the very edge of the strong-coupling region, it would not be surprising to find deviations from the rotational formula of Bohr and Mottelson,[46] and such deviations are easily noticeable. Take for

example the formula

$$E = (\hbar^2/2\mathcal{J})\ (I)\ (I+1),$$

which gives the energy, E, of a rotational state as a function of the spin of the state, I; we may use the energy of the 2+ state to fix the value of the moment of inertia, $\mathcal{J}$, and then calculate the energy of the 4+ state to be 412 kev. This is about 11% larger than is found. For nuclei in a comparable position in the strong coupling region of the very heavy elements, these corrections run as high as 23%. The above value of 11%, therefore, is not particularly disturbing.

The levels at 0.999 and 1.130 Mev are quite interesting. The spin of the 0.999-Mev level is very likely 2+, as has been discussed. If the moment of inertia were the same as for the ground-state rotational band, the 3+ member of the rotational band based on this level would be expected to be about 124 kev higher in energy. The 1.130-Mev level is 131 kev higher in energy, and furthermore the decay of this level to the 2+ and 4+ members of the ground-state band is consistent with its having a spin of 3+. For these reasons the two levels at 0.999 and 1.130 Mev are tentatively considered to be members of a rotational band with spins 2+ and 3+ respectively. This situation appears to be very similar to the levels in Pu^{238} populated by the beta decay of Np^{238}.[47] In this case two levels about 1 Mev above the ground state were observed which were assigned spins 2+ and 3+. From the radiations from these levels in Pu^{238} (which are all E2) it was possible to deduce that K, the projection of the spin on the nuclear-symmetry axis, was two for these levels. This in turn led to the suggestion that this rotational band might represent the gamma vibrational band predicted by Bohr and Mottelson to have these properties. The present case differs from Pu^{238} in that all the radiations from these levels do not seem to be E2. This could perhaps be due to the fact that Gd^{154} is on the very edge of the strong-coupling region, whereas Pu^{238} is well within this region in the heavy elements. Another possibility, which should not be entirely discounted, is that the multipolarity assignments are not correct. As was mentioned, the limits of error are sufficiently large that the assignments are only considered probable and not certain. The similarity of the two bands, however, and the observation of apparently analogous levels in other

heavy-element and rare earth even-even nuclei suggest that such bands might occur systematically throughout both strong-coupling regions.

One rather puzzling aspect of the Eu^{154} decay scheme shown in Fig. 19 is the large log ft values calculated for the beta transitions. The transitions to the ground-state rotational band of Gd^{154} have log ft values between 12 and 13, and this is perhaps understandable in that while ΔI is only one, ΔK is quite likely three for these transitions. Hence, so far as K is a good quantum number, these transitions would be second or higher forbidden. For the beta transitions leading to the 0.998- and 1.130-Mev levels, however, no such reason is evident. Here ΔI is probably one and zero respectively, and ΔK is probably one for both transitions. Depending on the parity of Eu^{154}, these should be allowed or first-forbidden transitions, and yet the log ft values are around 11. Since the spins of the other levels in Gd^{154} are not known, expected log ft values cannot be calculated. However, with a spin of Eu^{154} as low as 3, it is a little surprising that the smallest log ft value observed is 9. In terms of Ω-forbiddenness, which didn't seem to hurt much in Np^{238}, [47] these are all forbidden with a $\Delta \Omega = -3$. It may be that the $\Delta \Omega$ rules are more effective in this region, with the result that Eu^{154} has rather high log ft values.

III. DECAY OF EUROPIUM-155

A. INTRODUCTION

Eu^{155} should not have a complicated decay scheme compared with Eu^{154}, for the particles and gamma transitions reported in the literature on this nuclide are quite few. A year ago only two beta groups had been seen with energies of 250 and 150 kev and intensities of 77% and 23% respectively.[48,49] Recently Church[50] reported four beta components with the following beta end points, percentage intensity, and log ft.

Energy of Beta component (kev)	Intensity (%)	log ft
250	20	8.1
190	$\leq$ 10	$\geq$ 8.1
160	40	7.1
150	30	7.2

It is generally agreed that the 250-kev beta component decays directly to the ground state. The gamma transitions have been a bit more confusing than the beta groups. Rutledge et al.[51] reported gamma rays of 60, 87, 106, and 132 kev. In addition Lee and Katz[33] observed 18.7 and 136.8 kev from their conversion-electron studies, while Church and Goldhaber[28] did not see the 130-kev transition. So far three decay schemes have been proposed; namely by Wilson and Lewis,[48] Dubey et al.,[49] and Church.[50] The excited states by Wilson and Lewis were 85 and 100 kev, while those of Dubey et al. were 18 and 102 kev. From their experimental results they should have not been able to tell which is the first excited state, 18.8 kev or 85 kev. The common problem until now is the assignment of the 18.8 and the 86.5 kev in the decay scheme. Whether there is an 86.5-kev level or an 18.8-kev level in Gd^{155} is still unresolved, although Church's beta end-point data favor the 86.5-kev level. However, data from the beta end points alone may not be definitive in assigning the nuclear excited states, since their end points are separated by only about 10 kev. From coincidence measurements and energy summation the 86.5 and the 18.8 kev are in coincidence and originate from

the 105.2-kev level. It has been observed, both by Wilson and Lewis and by Dubey et al., that the 18.8-kev transition is a highly converted transition. From Coulomb excitation,[52,53] 60- and 145-kev levels in Gd^{155} belonging to the rotational band K = 3/2, odd parity, have been reported.

B. EXPERIMENTAL

1. Conversion-Electron Measurements

In this investigation of the conversion electrons of Eu^{155}, which was present in large numbers in the second sample of Eu^{154}, the conversion lines were calibrated against the 123.07-kev[30] transition conversion electrons of Eu^{154}. The conversion electrons assigned to Gd^{155} and their visual intensities are given in Table VIII. These were obtained with the same electron spectrographs[39] used in the studies of the decay of Eu^{154}.

2. Assignment of Multipolarities in the Transitions

From the conversion electrons whose energies are known to an accuracy of about 0.1% the gamma transition energies were calculated. The transitions assigned to gadolinium are 18.8, 41.60, 59.90, 86.50, 85.91, and 105.03 kev. Each one will be discussed in the succeeding sections and multipolarities assigned in the light of the relative intensities seen in the permanent-magnet beta-ray spectrographs and the theoretical conversion-electron coefficients calculated by Rose[45] and Sliv.[44]

18.8-kev transition. During the first short exposures this transition was not observed, due to its low intensity and because the film-detecting efficiency is poor in this energy range. However, other plates were exposed as long as possible without the beta spectrums producing a film blackening on the plate that makes reading the conversion lines impossible. All the three L lines were seen, and it is with great certainty that this 18.8-kev transition exists in Gd^{155}. Although not a very reliable multipolarity can be assigned to this transition, it seems that an E1 or an M1 (E2) mixture agrees with the observed intensities of the L lines. From Rose's theoretical L-conversion coefficients the L-subshell conversion-electron relative intensities are compared with the observed intensities:

TABLE VIII

Gamma-Ray Transition Energy (kev)	Conversion-Electron Energy (kev)	Shell Assignment	Conversion Electron Visual Relative Intensity I*	II**	Assigned Multi-polarity
18.80	10.40	L_I	vvw***	--	M1 (E2)
	10.86	L_{II}	vvw	--	
	10.53	L_{III}	vvw	--	
41.60	33.16	L_I	vw	--	E1 or M1 (E2)
	33.68	L_{II}	vw	--	
	34.35	L_{III}	vw	--	
59.9	9.67	K	vvw	--	M1 (E2)
	51.53	L_I	vvs	wm	
	51.95	L_{II}	m	vvw	
	52.56	L_{III}	vvw	--	
85.91	85.68	K	vw	--	E1 (?)
86.5	36.27	K	vvs	m	E1
	78.16	L_I	ms	m	
	78.54	L_{II}	w	vw	
	79.27	L_{III}	wm	wm	
	84.57	M_I	wm	vvw	
	86.01	N_I	vw	vvw	
105.2	54.97	K	vvs	s	E1
	96.70	L_I	ms	m	
	---	L_{II}	--	--	
	97.96	L_{III}	w	vvw	

* Film exposed for three days.

** Film exposed for one day.

*** The symbols mean: s, strong; m, moderate; w, weak; v, very.

Multipolarity	Relative Intensity $L_I:L_{II}:L_{III}$
E1	1.2:1.0:1.7
E2	0.005:1.0:1.4
M1	11.0:1.0:0.2
M2	19.5:1.0:10.5
Observed	vvw:vvw:vvw

Since the 105.2- and 86.5-kev transitions are to be proven to be positively E1 transitions, it seems reasonable to call the 18.8-kev an M1 (E2) transition, which the relative L-subshell ratios also suggest. When the L-conversion coefficients for the different possible multipole radiations are compared, an M1 plus E2 transition is the most converted multipolarity. This would agree with the experimental findings of Wilson and Lewis[48] and also of Dubey et al.[49] in which they concluded from their coincidence studies that the 18.8-kev transition is a very highly converted transition. The assignment of an M1 (E2) for this transition would also agree with Church's decay scheme, although he was not positive whether he saw such a transition in his conversion-electron results.

41.6-kev transition. The L_I, L_{II}, and L_{III} conversion electrons were observed for this transition and again with similar intensities, although the lines are more intense than the 18.7-kev. From Rose's theoretical L-conversion coefficients the L-subshell intensity ratios are:

Multipolarity	Relative Intensity $L_I:L_{II}:L_{III}$
E1	2.4:1.0:1.4
E2	0.02:1.0:1.3
M1	12.0:1.0:0.2
M2	12.0:1.0:4.5
Observed	vw:vw:vw

which shows that this can either be an M1(E2) mixing or a pure E1 transition. From energy differences this transition does not fit very well the transition between the 145.8-kev and 105.2-kev level. The 145.8-kev level energy was based only on the energy of the K line of the 85.91-kev

transition, and it is the second excited state of the rotational band. This 146 level was observed by Bjerregaard and Meyer-Berkhout[52] and also by Heydemburg and Temmer[53] in their Coulomb excitation experiments. It will be shown later that the beta group feeding the 146-lev levels is quite small and that it would escape detection in the study of the beta spectrum of Eu^{155}.

For reasons to be discussed shortly, there are a few inconsistencies in this transition; therefore, it was not placed in the decay scheme. First of all, if the first excited state of Gd^{155} is 18.8 kev and not 59.9 kev, 41.6 kev is just the right transition energy-wise from the 59.9- to the 18.8-kev level. The necessary multipolarity assignment would also agree with the experimental intensities, which would be an M1 (E2) for this case. The conversion-electron data support the 18.8-kev as the first excited state of Gd^{155}.

In both cases the 41.6-kev can be the transition between the 145.8- and the 105.2-kev levels of Gd^{155}. Hence the 41.6-kev should be an E1. If the 41.6-kev is an E1 and the 85.91-kev is an M1, their conversion coefficients are 0.01 for the L_I and 3.5 for the K of 41.6 and 85.91 kev respectively. Therefore the gamma intensity of the 41.6-kev should be about 300 times as intense as that of the 85.9-kev for this multipolairty assignment to be correct. Such is not the case experimentally, for they seem to have the same intensity. In the Coulomb excitation experiments, only the 86-kev gamma was seen coming from the 146-kev level. However, the 41.6-kev is in the K x-ray region of gadolinium, which is 41.8-kev; that would make its detection difficult. From the gamma-spectrum curve of Heydenburg and Temmer the presence of the 41.6-kev cannot be completely discounted because of their intense K x-ray peak.

The presence of this transition strongly supports the presence of an 18.8-kev level and puts some doubt on the validity of the beta end points of Church.[50]

59.90-kev transition. Before the results on Coulomb excitation were published it was perplexing to note the presence of a strong transition of 59.90 kev, which was hard to fit into the then known decay scheme of Eu^{155}, especially when the gamma spectrum did not see the presence of any 60-kev transitions and some investigators did not find

this transition. However, its presence was positively due to either Eu^{155} or Eu^{154}, since the sample contained nothing more, as shown by mass analysis. Fortunately this state was also excited by Coulomb excitation[52] and is the first excited state of the rotational-band spectrum of Eu^{155}. The relative subshell intensities are:

Multipolarity	Relative intensity $L_I:L_{II}:L_{III}$
E1	3.2:1.0:1.3
E2	0.05:1.0:1.1
M1	11.1:1.0:0.2
M2	10:1.0:1.0
Observed	wm:vvw: - vvs:m:vvw

The fact that the L_{III} was not seen in the short exposure runs strongly suggests an M1 transition. However, it is reasonable that there is also at E2 mixture in this transition. Church and Goldhaber[28] calculated this amount of mixing to be 94% M1 and 6% E2 from the conversion coefficients of Rose[45] and his conversion electron intensities, which agrees with this investigation. From Coulomb excitation[52] a 5% E2 mixture was reported. Furthermore the possibility of the 59.90-kev's being an E1 is discounted by the fact that it was excited by Coulomb excitation, which so far, with the exception of the weakly excited 109-kev level in F^{19}, has produced only E2 transitions.[54]

86.50-kev transition. In terms of conversion-electron intensities this is the strongest transition observed in Gd^{155}. From the relative subshell intensities below,

Multipolarity	Relative intensity $L_I:L_{II}:L_{III}$
E1	4.1:1.0:1.1
E2	0.2:1.0:0.05
M1	11.3:1.0:0.2
M2	9.0:1.0:2.0
Observed	m : vw : wm ms : w : wm

the only possible transition multipolarity is E1 or M2. Rutledge et al.[51] assigned this as an E2 transition based on their K/L ratio of 8.0 ± 2.8. Lee and Katz[33] found the K/L ratio to be four. From Sliv's K-conversion coefficient and Rose's L-conversion coefficients corrected for screening, the conversion coefficients for the possible multipolarities are presented:

TABLE IX

Multipolarity	Conversion Coefficients					Relative Intensity
	K	L_I	L_{II}	L_{III}	L_{Total}	K/L
E1	4.0	0.5	0.03	0.005	0.54	7.4
E2	28.0	6.5	0.7	1.4	8.6	3.3
M1	0.4	0.04	0.01	0.01	0.06	6.7
M2	1.3	0.2	1.1	1.1	2.35	0.6

The only conclusion from the K/L ratio is that this transition cannot be an E2 transition. The possible assignments are M1, M2, or E1, but as will be proved shortly this 86.50-kev cannot be a magnetic transition, and hence the only possible multipolarity is an E1.

The proof is as follows: If the 105.2-kev is an E1 transition, an independent check of the multipolarity of the 86.5-kev can be calculated using the gamma spectrum of Dubey et al.[49] The relative intensities of the 42-kev gadolinium K x-rays, and 84-kev and 102-kev photopeaks were measured with a planimeter, corrected for crystal efficiency and iodine escape peak. The results are:

Energy of Gamma Ray (kev)	Relative Intensity (arbitrary units)
42 K x-rays	14.9
84	16.3
102	9.8

The K fluorescence yield of gadolinium from Gray's[43] curve is 0.93, and hence the electron intensity of all the transitions above 50 kev is 16.0. The K-conversion coefficient for an E1 transition of 102 kev energy is 0.24, and hence the K-conversion-electron intensity is 3.8. Assuming that the conversion-electron contributions of the other transitions are small compared with the 84-kev and 102-kev transitions, an upper limit for the K-conversion-electron coefficient of the 87-kev transition can be

calculated, and this turns out to be 0.75. From Sliv's K-conversion coefficients for an 86-kev transition the theoretical values are:

Multipolarity	K-conversion coefficient
E1	0.22
E2	0.92
M1	1.6
M2	13.0
Observed	$\leq$ 0.75

The results show that the 84-kev is either an E1 or an E2 but cannot be an M1 or an M2. However, the relative L-subshell conversion-electron intensities limit the possible multipolarities only to an E1 or M2. Hence by combining the interpretations obtained from the gamma intensities and the L-subshell intensities it can be concluded that the 86.50-kev is an E1 transition.

Another way of looking at this is to assume that all the electron intensity of 16.0 is due to the K-conversion electrons of the 86.5-kev transition. In this way the maximum K-conversion coefficient of the 86.5-kev transition amounts to 0.98. Hence it eliminates without any doubt the possibility that the 86-kev is a magnetic transition; more so if it is an M2 transition. Similarly we can calculate the maximum K-conversion coefficient for the 105.2-kev transition, assuming that all the electron intensity 16.0 is due to its K-conversion electrons. From this assumption, $\alpha_K \leq 1.6$ for the 105.2-kev transition.

The K-conversion coefficients as given by Sliv for the 105-kev transition are:

Multipolarity	Conversion coefficient
E1	0.2
E2	1.0
M1	1.7
M2	10.0
Observed	$\leq$ 1.6

Hence, the probability that the 105.2-kev in an M2 transition is very small, a reasoning which would be used shortly.

By comparing the intensities of the K-conversion lines of the 105.2- and 86.5-kev transitions, which are supposed to be both E1, a

glaring inconsistency was noted in the permanent-magnet spectrograph plates. Since the 87-kev is more intense gamma-wise, it should be expected that the K lines of the 87-kev should be stronger than the K line of the 105.2-kev; but it was not so. This can only be true if the 105.2-kev K line is composed of conversion lines from two or more different transitions or if the multipolarity assignments are incorrect. Fortunately these two K peaks were strong enough to be seen in the beta spectrum obtained from the magnetic spectrometer, and their relative intensities can be compared after subtracting the beta background. The results are:

Transition	K-conversion-electron intensity (arbitrary units)
86.4 kev	7.4
105.0	6.4,

which is in agreement with the assignment of both the 86.5- and 105.2-kev to E1 transitions. Incidentally, this may show the limits of accuracy in reading relative intensities by visual comparison.

105.2-kev transition. This is in coincidence with the 150-kev beta component, and is the cross-over transition of the 18.8- and 86.5-kev transitions. From the relative intensities of the L-subshell conversion electrons and Rose's[45] conversion-coefficient data the multipolarity possible for the 105.2 is either an E1 or an M2, as seen below:

Multipolarity	Relative Intensity $L_I:L_{II}:L_{III}$
E1	4.7:1.0:1.2
E2	2.1:1.0:1.0
M1	1.3:1.0:1.9
M2	9.0:1.0:1.9
Observed	ms : - : w
	m : - : vvw

However, based on the conclusions derived from the gamma-ray intensities of Dubey et al., the possibility of an M2 transition for the 105.2-kev is entirely discounted, leaving only the E1 as the logical assignment for this transition, and is in agreement with all the experimental data.

145-kev transition. Heydenburg and Temmer[53] observed this transition in their Coulomb excitation of Gd^{155}. However, in the conversion-electron studies no evidence of the 145-kev transition was

observed. This would lead one to believe that it is not being populated very heavily from the beta decay of Eu^{155}, which is what the beta-component results show.

3. Decay Scheme

The proposed decay scheme for Eu^{155} is given in Fig. 20. The ground state of Gd^{155} is assigned as 3/2 from the work of Jenkins and Speck,[55] and a negative parity from the magnetic-moment results of Speck.[56] It is the first level of the rotational band K = 3/2- as deduced from the Coulomb excitation experiments. Using Nilsson's[57] diagram for highly deformed nuclides, the most logical assignment for this level is $\Omega = 3/2 = I$, $K = 3/2$, $\pi = -$, $N = 5$, $n_z = 2$, and $\Lambda = 1$, or in short as 3/2-, [5,2,1].

Since the 59.9-kev transition is mostly an M1 transition, the first excited level of the rotational band should have a spin of 1/2, 3/2, or 5/2 and odd parity. However, it is known that this is the first excited state of the rotational band and therefore is the $I = 5/2$, $K = 3/2$, $\pi = -$, $N = 5$, $n_z = 2$, and $\Lambda = 1$, which agrees with the experimental results. Also, the beta intensity of $\leq$ 10% is in agreement with the theoretical prediction of Alaga et al.[58] for beta transitions to members of a rotational band. If this is the 5/2, 5/2- state we can calculate the second excited state of the rotational band using Bohr and Mottelson's[46] formula, and the predicted 7/2, 3/2- state is 145.2 kev. The presence of such a state has been confirmed by Coulomb excitation and the transition between the 145.8-kev and the 59.9-kev has been seen in this investigation. As for the 145.8-kev transition, it was observed only in Coulomb excitation. It was not surprising to note the absence of the 145.8-kev transition in the conversion-line spectrum, since its reduced transition probability is 3.8 times as small as the 85.9-kev and also 7.5 times less converted. So, the rotational band structure of Gd^{155} is well established and the assignments well substantiated.

The 105.2-kev and 86.5-kev levels are fed directly by the two allowed hindered beta-decay types, and hence the reason for their higher intensities. Although the 86.5-kev state is still open to question, it seems that the beta end points of Church[50] are of sufficient accuracy

and confidence to believe that such a level exists. Furthermore, if we compare $^{91}_{64}Gd^{155}$, which has 91 neutrons, with $^{140}_{91}Pa^{231}$, which has 91 protons, a striking similarity is evident. The lower levels of Pa^{231} are tentatively known as 0, 58.5, 84.1, 101.3, and 165.2 kev, and that of Gd^{155} are 0, 59.9, 86.5, 105.2, and 145.8 kev. How far the correlation can be carried is questionable. Since the 105.2-kev is an E1, the 105.2-kev level should be of even parity and the spins could be 1/2, 3/2, or 5/2.

The 41.6-kev can only be an E1 or an M1 (E2) mixture. Now that it is known that the 105.2-kev has even parity, the 41.6-kev should be an E1. But what is important is that the change in I can only be one or zero for both possible types of transitions from the I = 7/2 level. The 86.5-kev level can be either I = 1/2, 3/2, or 5/2, and even parity from the E1 nature of the 86.5-kev transition. Since the 18.8-kev is an M1 (E2) transition, the only possible assignment to the 86.5-kev transition which agrees with experiment is a spin of 3/2 and even parity. From the possible configurations in the Nilsson diagram agreeing with these spins and parities are sought the most logical assignments, which are 5/2, +,6, 4, 2 and 3/2,+,6, 5, 1 for the 105.2- and 86.5-kev levels respectively.

The final assignments of levels is shown in Fig. 20, and a test of their correctness would be shown in the discussion of the beta components.

The log ft of the beta components are rather high if based on the Gamow-Teller selection rules. However, these unusually high log ft values are explained when we use Alaga's[59] selection rules. The ground state of Eu^{155} was assigned the Nilsson state 5/2, +,4, 1, 3, based on its known spin. The analysis as shown in Table X classifies all the transitions as based upon the Nilsson states to be hindered, and hence the reason for the slightly higher log ft values.

Using Alaga et al.'s[58] transition probabilities to members of a rotational band, the squares of the Clebsch-Gordan coefficients, C^2, were calculated for $K_i = 5/2$ to $K_f = 3/2$, 5/2, and 7/2 with $\Delta \ell = 1$. With 20% (assumed) intensity for the ground state, the theoretical beta intensities for the excited states of the rotational band were calculated. Since the square of the Clebsch-Gordan coefficients[60] are not energy-dependent, these were corrected, and the results are given in Table XI.

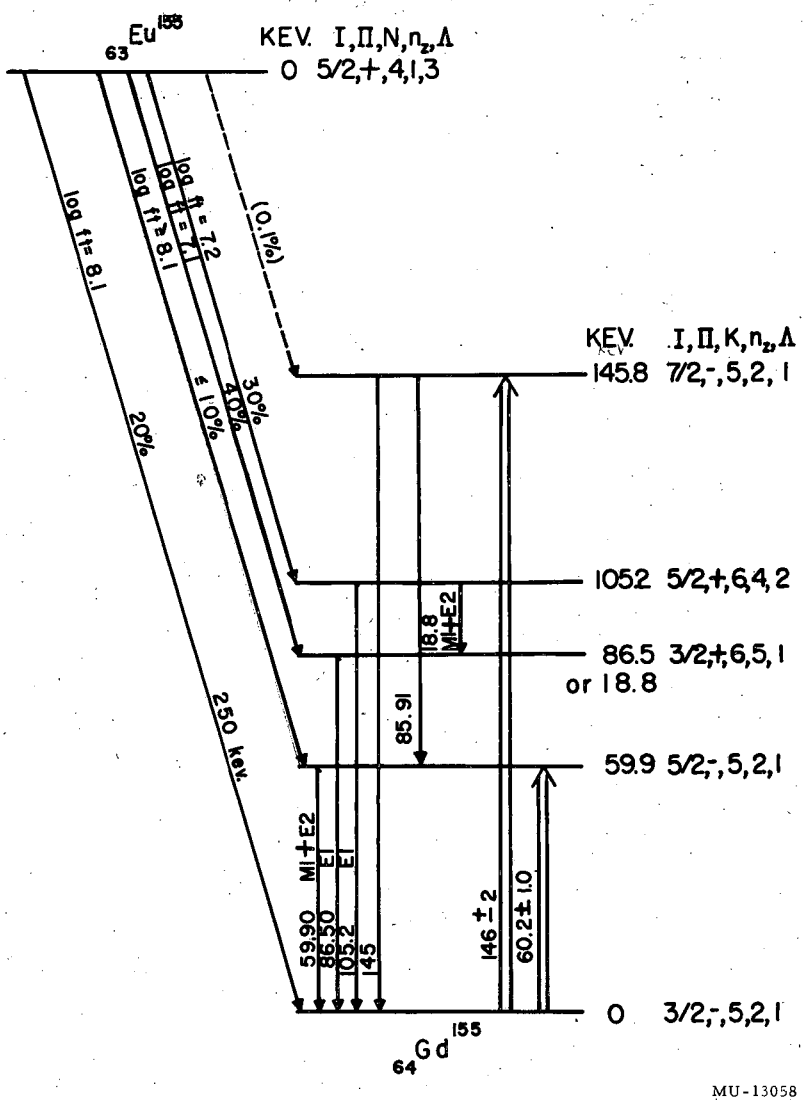

Fig. 20. Decay scheme of Eu^{155}.

TABLE X

Analysis of the Beta Transitions

Final State (kev)	Δ I, $\Delta \pi$, Type	Δ K, Δ N, Δn_z, $\Delta \Lambda$	Asymptotic classification	Experimental log ft Data	
				Church	Rutledge et al.
145.8	1, yes, 1st forbidden	1, 1, 1, 2	Hindered	--	--
105.2	0, no, allowed	0, 2, 3, 2	Hindered	7.2	6.8
86.5	1, no, allowed	1, 2, 4, 2	Hindered	7.1	--
59.9	0, yes, 1st forbidden	1, 1, 1, 2	Hindered	$\leq$ 8.1	--
18.8	1, yes, 1st forbidden	1, 1, 2, 1	Hindered	--	--
0.0	1, yes, 1st forbidden	1, 1, 1, 2	Hindered	8.1	8.1

TABLE XI

Beta End point	Final State	Without energy-dependence correction		Corrected for energy dependence		Experimental Relative intensity
		C^2	Relative intensity	C^2/t	Relative intensity	
250 kev	3/2, 3/2-	0.667	(20%)	(0.667)	(20%)	20%
190	5/2, 3/2-	0.285	9%	0.190	6%	$\leq$ 10%
104	7/2, 3/2-	0.048	1.4%	0.007	0.2%	--

The agreement between theory and Church's experimental intensities is remarkable, and this explains why the 104-kev beta group was not seen. It is noteworthy to mention also that the 86.5-kev transition, owing to its very strong intensity, cannot be used as the transition between the second and first excited states of the rotational spectrum, although its energy would be right for such a transition.

IV. DECAY OF THORIUM-231

A. INTRODUCTION

Th^{231}, known first as UY, the daughter of U^{235}, was first prepared by Jaffey and Hyde[61] by Th^{230} (n,γ) Th^{231}. It is a beta-emitter with a half-life of 25.6 hours. The beta spectrum was studied by Freedman at al.,[62] and in it they reported the following beta components: 302 ± 2, 216 ± 5, and 94 ± 2 kev with relative intensities of 44%, 11%, and 45% respectively. From their results a large amount of error in the relative intensities is evident, since the electron spectrometer they used did not have enough resolution to resolve the lower-energy conversion-electron lines. Furthermore, they would fail to separate other beta groups whose end points would fall in this region. Inconsistencies appeared in that there were far too many more beta transitions in the 94-kev group than can be accounted for from the gamma-ray intensities coming from the state populated in their proposed decay scheme. Also the experimental log ft value was too low for the 94-kev beta component.

Recently Mize and Starner[63] restudied the conversion-electron lines of Th^{231} beta decay, but they used the results of Freedman et al. for the beta end points and their relative intensities.

B. EXPERIMENTAL

1. Beta components of Th^{231}

Hollander, Asaro, and Stephens[64] produced Th^{231} by (n,γ) reaction and studied this nuclide using permanent-magnet electron spectrographs and gamma scintillation counters. In conjunction with this work the energies of the beta end points and the relative intensities of the conversion electrons and beta components were determined using a double-focusing semicircular electron spectrometer[11,40] with a thin-window Geiger-Muller counter as the detector. The resolution of the instrument was 0.5%. Several runs of the beta spectrum were made and the half-life of the sample was followed in order to detect any impurity present in the sample. All these checks showed the sample to be pure, and the shape of the beta spectrum was reproducible even after several half-lives. In this all the stronger conversion lines were beautifully resolved, and

enough events were taken to assume that the error in the beta-spectrum shape is small. The sample had an activity as read from a JUNO* Model 3 of 50 R at a distance of half an inch when the source was introduced into the spectrometer. The following beta components were resolved with straight lines using a Fermi-Kurie plot (Fig. 21) which indicates that the transitions are all allowed.

TABLE XII

Beta Components of Th^{231} Decay

Maximum energy of beta (kev)	Relative Intensity (%)	Experimental log ft
299 ± 2	38.5	6.0
218 ± 4	33.3	5.6
134 ± 6	20.0	5.2
90 ± 8	8.2	5.2

No beta group higher than 299 kev was seen, and if there is any it should be present with a relative intensity of less than 0.1%. From coincidence measurements[65] the strongest beta component feeds the 84-kev level, which has a half-life of 4.1×10^{-8} second. The Fermi-Kurie plot is given in Fig. 21 and the corresponding beta spectrum as reconstructed from the Fermi-Kurie diagram is given in Fig. 22. As a final check the original beta spectrum was normalized to fit the sum of the intensities of the four beta-spectra groups derived from the Fermi plot, and the agreement was satisfactory except in the lower energy range, where the window-absorption correction had to be applied to the original beta spectrum.

2. Relative Intensities of the Conversion Lines and Their Multipolarities

The conversion electron peaks were measured with a planimeter to compare their relative areas after they were assigned to their corresponding gamma transitions. With the simple assumption that their areas are proportional to their intensities, the relative ratios of the subshell conversion electrons can be expressed by numerical values. The multipolarities of the more intense transitions were assigned, based on

* Made by Technical Associates, 140 West Providencia Avenue, Burbank, California.

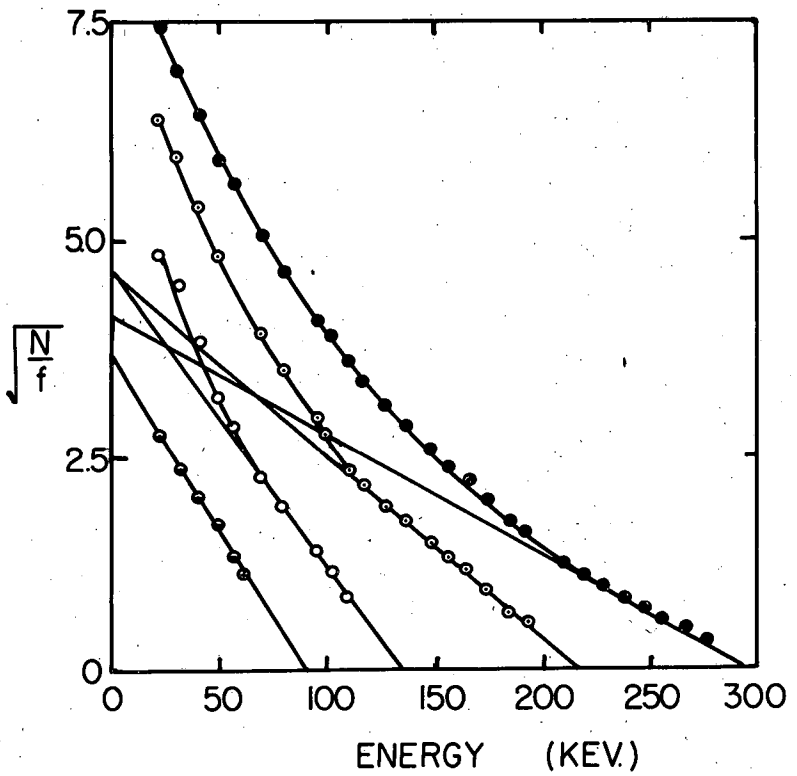

Fig. 21. Fermi plot of the beta spectrum of Th^{231}, showing resolution into components.

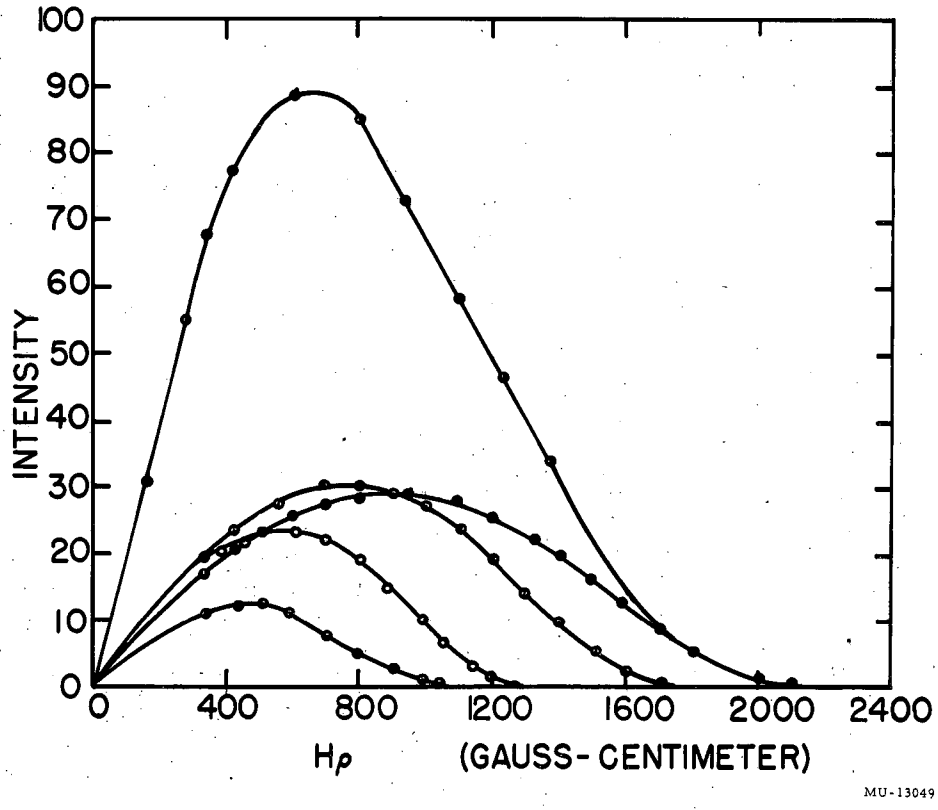

Fig. 22. Beta spectrum of Th^{231} as reconstructed from the Fermi-Kurie plot of Fig. 21.

the theoretical values for the conversion-electron coefficients of Rose et al.[45] for the L and M subshells and the values of Sliv[44] for the K-conversion electron coefficients.

The results, with an accuracy of about 20%, are given in Table XIII, where the intensities of seven runs are normalized. Greater accuracy of intensity ratios is obtained when comparing intensities in the same run. Hence in all discussions dealing with L and M subshell intensity ratios, the intensities obtained in the same run are used. The energies and shell assignments are from Hollander et al.[64]

Since there were quite a few low-energy conversion-electron lines in this nuclide, window corrections should be made when their relative intensities are compared. To find out the percentage transmission, or more correctly expressed, the counting efficiency of the G-M counter as a function of electron energy, the beta spectrum of Pm^{147} was run with the same conditions in the magnetic spectrometer. The Fermi plot was made, and from the deviations from the straight-line plot at the lower energy range the correction factor expressed as percent transmission was calculated. It must be understood that the correction factor includes all causes like charging effect, hysteresis counting effect, gas composition, high voltage, etc., in addition to the absorption and scattering effects of the plastic window, which was VYNS - 3 in this experiment with a thickness of about 15 micrograms per cm^2. The results are plotted in Fig. 23, and the corrections were applied to the data in Table XIII. From previous investigation using different types of films but of the same thickness, similar results were obtained for the correction factors.

Each of the stronger transitions is to be discussed individually in detail in the succeeding sections.

17.2-kev transition. Since only the M_{III} line was strong enough to be seen in the magnetic spectrometer, no reliable multipolarity can be assigned to this transition. The theoretical and observed M-subshell conversion-electron intensity ratios are:

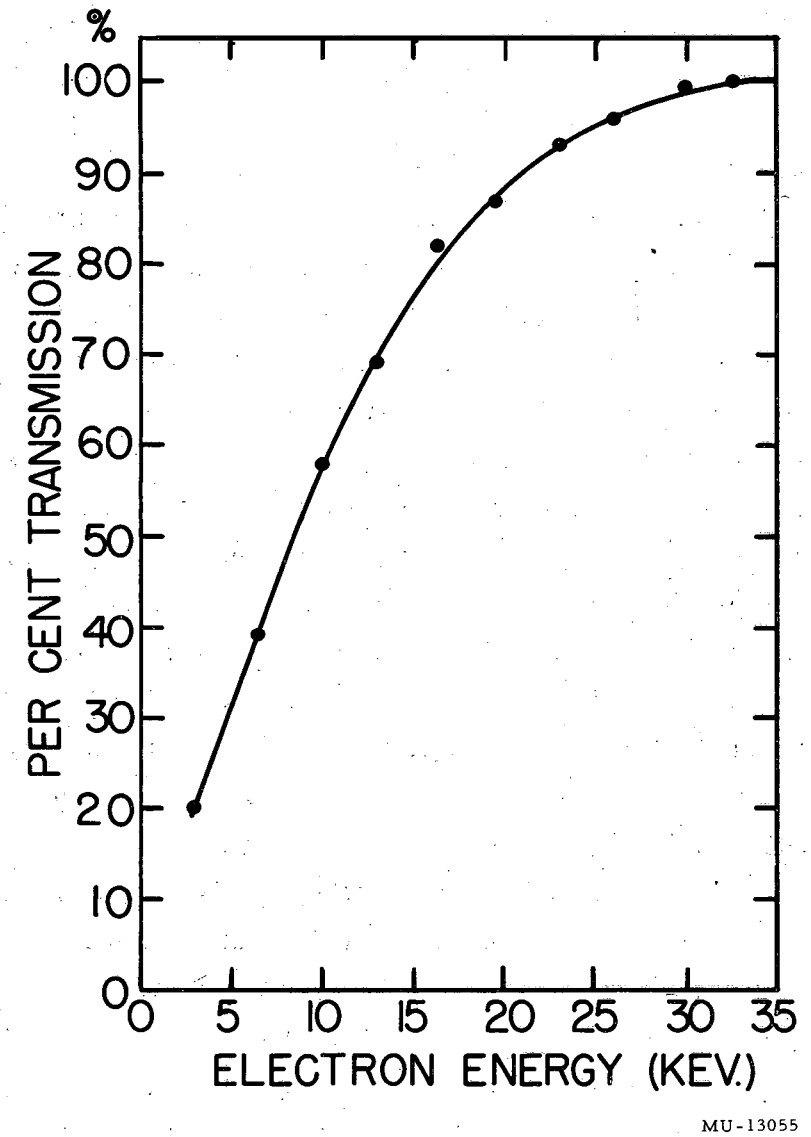

Fig. 23. Electron-counting efficiency of the G-M counter of the magnetic spectrometer calculated from the Pm^{147} beta spectrum.

TABLE XIII

Conversion Electrons of Th^{231}

Multi-polarity	Tran-sition Energy (kev)	Conversion Electron Energy (kev)	Assign-ment	Relative Intensities							Normalized Relative Intensities
				1	2	3	4	5	6	7	
E1?	17.20	11.83	M_I	--							--
		12.22	M_{II}	--							--
		13.06	M_{III}	2.0						3.1	6.1
		15.84	N_I								
		15.98	N_{II}	12.9						5.6	4.0
		16.21	N_{III}	(~3.1)							(~1.0)
E1	25.63	20.29	M_I	12.9	7.3						4.0
		20.65	M_{II}	13.8	7.5						7.3
		21.46	M_{III}	18.4	11.7	7.1					5.9
		22.03	M_{IV}	5.0	3.8	3.8					1.5
		22.20	M_V	5.7	2.0						1.7
		24.24	N_I			1.7					1.4
		24.39	N_{II}		7.9	1.8					1.5
		24.60	N_{III}			1.6					1.4
		24.90	N_{IV} N_V		2.3	1.5					1.3
		25.39	O		1.9	1.1					0.8

TABLE XIII (continued)

Multi-polarity	Transition Energy (kev)	Conversion Electron Energy (kev)	Assignment	Relative Intensities 1	2	3	4	5	6	7	Normalized Relative Intensities
E2	58.47	37.36	L_I								--
		38.24	L_{II}				21.7				100
		41.80	L_{III}				20.4				94
		53.55	M_{II}				7.7				35.4
		54.33	M_{III}				4.5				20.8
		54.83	M_{IV}				--				--
		57.24	N_{II}			16.2	3.7				17.1
		57.45	N_{III}								
		57.65	N_{IV}			--	--				--
		58.26	O_{III}			7.4	1.1				5.1
		58.42	P			--	--				--
E2	68.46	48.14	L_{II}			1.0					$0.8^{(0.7)}$
		51.70	L_{III}			0.3					$0.3^{(.2)}$
		64.36	M_{III}			--					--
M1 (E2)	81.10	60.06	L_I				5.3				24.4
		75.73	M_I					9.3	2.5		5.6
		76.06	M_{II}					1.5			0.9
		79.74	N_I					3.8			2.4

TABLE XIII (continued)

Multi-polarity	Transition Energy (kev)	Conversion Electron Energy (kev)	Assignment	Relative Intensities 1	2	3	4	5	6	7	Normalized Relative Intensities
M1 (E2)	81.95	60.89	L_I			12.2	2.7				10.0
		61.66	L_{II}			1.4					1.2
		76.60	M_I					4.7	1.3		2.9
		76.90	M_{II}					2.1			1.3
		80.55	N_I					--			--
		80.81	N_{II}					1.6			1.0
E1	84.09	63.07	L_I				7.8				35.9
		63.81	L_{II}			20.4	3.1				14.3
		78.76	M_I						6.0		13.4
		79.08	M_{II}					7.3			4.5
		79.89	M_{III}								--
		80.55	M_{IV} M_V						0.4		0.5
		82.70	N_I						1.4		3.1
		82.88	N_{II}					7.1			1.3
		83.80	O					1.5			
M2	99.28	78.05	L_I					5.4	2.3		5.2
		82.46	L_{III}					1.0			0.6
		93.94	M_I					1.0			0.6

TABLE XIII (continued)

Multi-polarity	Transition Energy (kev)	Conversion Electron Energy (kev)	Assignment	Relative Intensities 1	2	3	4	5	6	7	Normalized Relative Intensities
M2	99.28	94.29	M_{II}								--
		95.22	M_{III} (+?)								--
		97.98	N_I								--
M1 (E2)	135.7	23.1	K		1.3						0.8
		114.6	L_I					1.3			0.8
		115.4	L_{II}								--
		130.4	M_I								--
	163.3	50.46	K			1.3			0.6		1.1

Transitions not seen in the magnetic spectrometer:

63.75 kev

75.93 kev

89.76 kev

146.0 kev

Multipolarity	M-subshell relative intensity
E1	0.4:0.7:1.0
E2	0.04:0.9:1.0
M1	200:16.5α1.0
M2	3800:0.007:1.0
Observed	- : - : 1.0

where a dash means it was not observed in the magnetic spectrometer, due to its weak intensity. Although no definite multipolarity assignment can be deduced, a reasonable one can be made and some impossible multipolarities eliminated. From the above data M1 and M2 can be disregarded in future considerations of this transition. Comparing E1 and E2, the E1 seems to fit more the observed results while an M1 (E2) mixture seems hardly possible.

It would be nice to have available also N-subshell conversion-electron coefficients in order that a more reliable multipolarity could be given to this transition. The $(N_I + N_{II}) / N_{III}$ ratio of 3 obtained for this transition would be a good check when the N-subshell conversion-electron coefficients were calculated, and also it would give more confidence in pinning down the multipolarity assignment of the 17.2-kev transition.

25.6-kev transition. The assignment of this transition was based on the conversion lines seen in the permanent-magnet spectrographs, which were the L_{III}, M_I, M_{II}, M_{III}, M_{IV}, M_V, N_I, N_{II}, N_{III}, N_{IV}, and N_V, and O conversion electron lines. All of these were also seen in the magnetic electron spectrometer, with the exception of the L_{III}, and the relative intensities calculated. Strominger and Rasmussen[65] reported this transition to be in coincidence with the highest-energy beta group, and with a lifetime of 4.1×10^{-8} second. This information eliminates transitions of only $\Delta I = 3$ or higher orders.

The experimental and theoretical relative intensities of the M-subshell conversion-electron lines are as follows:

Multipolarity	Relative Intensities $M_I:M_{II}:M_{III}:M_{IV}:M_V$
E1	0.6:0.7:1.0:0.4:0.5
E2	0.03:1.0:1.0:0.02:0.01
M1	163:18.2:1.0:0.1:0.07
M2	1.7:0.8:1.0:0.2:0.01
Observed	0.6:0.6:1.0:0.3:0.2 0.7:0.7:1.0:0.3:0.3

All the M-subshell relative intensities were calculated from the unscreened conversion-electron coefficients of Rose. Although the absolute values of the actual conversion coefficients would be lower owing to the screening correction, the relative intensities of the M-subshell conversion electrons should remain the same, and hence the interpretations in this study would still be valid.

It is unmistakably an E1 transition, and all the other types are eliminated from the results. Two experimental values are given to show the reproducibility of the intensities, although in the succeeding sections only one number would be given.

58.47-kev transition. Compared with the other transitions this has more ways by which the multipolarity can be determined because the L and M subshell ratios were obtained. In addition it is the strongest transition in terms of conversion-electron intensities. The relative intensities of the subshell-conversion electrons are given below and compared with the theoretical ratios.

	Multipolarity	$L_I:L_{II}:L_{III}$	$M_I:M_{II}:M_{III}$	L:M
Theoretical	E1	1.1:1.0:1.0	1.3:1.0:1.1	1.1:1.0
	E2	0.04:1.0:0.9	0.05:1.0:0.8	2.2:1.0
	M1	10.9:1.0:0.04	85:1.0:0.04	3.1:1.0
	M2	136:1.0:52	10.6:1.0:4.7	2.2:1.0
Observed		- : 1.0 : 0.9	- : 1.0 : 0.6	3.5:1.0

From the relative subshell ratios of the L and M-conversion electrons it is clearly proven that this transition is an E2 transition. A dash in the experimental result means that the conversion electrons may be present in the beta spectrum, but the intensity is such that their

presence was not evident in the midst of the beta spectrum. A rough approximation giving this intensity as around 0.05 would agree well with the theoretical prediction for an E2 transition.

As for the L/M ratios it is difficult to say much from the results obtained, since the ratios are not sensitive enough to eliminate one type of multipolarity over the other. And even when the M-conversion electron coefficients were corrected for screening the difference between one multipolarity and another in the L/M ratio would be within the experimental error.

The presence of the 58.5-kev level has been confirmed by Coulomb excitation,[66] and agrees with the assignment of an electric transition.

68.5-kev transition. This is the only other electric transition where a $\Delta I = 2$ is suggested from the L-subshell conversion-electron intensities. Although it is difficult to fit it into the decay scheme of Hollander et al.,[64] still its intensity is such that a multipolarity can be assigned to it with certainty. The theoretical and experimental values are:

Multipolarity	Theoretical subshell ratios $L_I:L_{II}:L_{III}$
E1	1.3:1.0:1.0
E2	0.04:1.0:0.8
M1	10.7:1.0:0.04
M2	126:1.0:4.1
Observed	- : 1.0 : 0.3

As in the previous cases, any time the intensity was about 0.04 compared to 1.0, where 1.0 is barely seen, such a conversion electron is not seen in the spectrometer. No other transition agrees with the experimental result other than the E2 transition. Hence, for future consideration of this transition in the decay scheme, it should be in agreement with a multipolarity equivalent to an E2 transition. However, a possibility of a very small M1 mixed with the predominantly E2 transition should not be discounted.

81.1-kev transition. The theoretical and experimental relative intensities of the M subshell conversion electrons are:

Multipolarity	Relative M-subshell Intensities
E1	1.5:1.0:1.0
E2	0.06:1.0:0.8
M1	8.8:1.0:0.04
M2	6.2:1.0 -
Observed	6.2: 1.0: -

The data clearly suggest an M1 (E2) mixing. Using the $M_I:M_{II}$ ratio, a crude estimate of the E2 admixture in this transition was calculated and found to be about 30%.

81.85-kev transition. The theoretical and experimental L- and M-subshell conversion-electron ratios are:

Multipolarity	Theoretical Relative Intensities	
	$L_I:L_{II}:L_{III}$	$M_I:M_{II}:M_{III}$
E1	1.7:1.0:1.0	1.5:1.0:1.0
E2	0.05:1.0:0.7	0.06:1.0:0.8
M1	11.7:1.0:0.04	8.8:1.0:0.04
M2	10.0:1.0:3.7	9.0:1.0:3.6
Observed	8.7:1.0: -	2.2:1.0: -

It agrees with an M1 (E2) mixing of almost equal amounts. From the L-subshell ratios a mixing of 70% M1 to 30% E2 is obtained, while the M-subshell ratios need a 70% E2 and 30% M1. Hence, in the calculation of the transition intensities, a 50-50 mixing would be assumed for this transition.

84.09-kev transition. In the preceding sections the 58.5- and 25.6-kev transitions were definitely assigned their multipolarities as E2 and E1 respectively. Hence the choice of the 84.1-kev transition, if it is the cross-over transition, should be one with a change of parity. The theoretical and experimental L- and M-subshell ratios are given below:

Multipolarity	Theoretical Relative Intensities $L_I:L_{II}:L_{III}$	$M_I:M_{II}:M_{III}$
E1	1.7:1.0:1.0	1.6:1.0:1.0
E2	0.05:1.0:0.7	0.06:1.0:0.8
M1	11.7:1.0:0.04	8.3:1.0:0.04
M2	10.0:1.0:3.7	9.0:1.0:3.5
Observed	2.5:1.0: -	3.0:1.0: -

The L and M-subshell electrons suggest either an E1 or an M1 (E2) mixture, although an M1 (E2) with 70% E2 would fit the experimental data better. Now this introduces a conflict with the expected change of parity, and can be resolved only if it is assumed that there are two transitions of the same energy, 84.1 kev, one of which is an E1; or this transition is an E1 and not an M1 (E2); or that the 84.1-kev is not the cross-over transition of 58.5 and 25.6 kev. The most logical step to take is to say that the 84.1 is an E1 transition within experimental accuracy, since the probability of having two transitions of exactly the same energy in the same nuclide or of a transition whose energy equals exactly the sum of two other transitions but which is not the cross-over transition is small. Furthermore, there has been recently a number of supposedly E1 transitions whose relative intensities do not agree with the theoretical relative intensities and have been referred to as "abnormal E1 transitions."[67] All these suggest that the most reasonable assignment for the 84.1-kev transition is an E1, since it fits the whole experimental data better. However, as would be shown later, this introduces some doubts as to its true E1 nature.

99.3-kev transition. The theoretical and observed relative intensities of the L-subshell conversion electrons are:

Multipolarities	Relative Intensities $L_I:L_{II}:L_{III}$
E1	2.0:1.1:1.0
E2	0.09:1.5:1.0
M1	275.0:25.0:1.0
M2	3.7:0.4:1.0
Observed	5.4: - :1.0

It seems to show that the 99.3-kev is an M2 transition, from the L-subshell intensities. However, it would be safer if there would be other means to determine this multipolarity independently, although in this report it would be treated as an M2 transition.

135.7-kev transition. Only the K- and L_I-conversion electron lines were seen for this transition and at two different runs, so only a crude assignment would be made. Upon normalizing their relative intensities one discovers that they are present in the same abundance. The relative intensities of the K- and L_I-conversion electrons using Sliv's conversion coefficient for the K line and Rose's conversion coefficient for the L_I line are given below:

Multipolarity	Conversion Coefficient K	Conversion Coefficient L_I	Relative Inteisity K/L_I
E1	0.19	0.02	7.9
E2	0.24	2.0	0.1
M1	6.6	3.7	1.8
M2	30.0	2.3	13.0
Observed			1.0

From the K/L_I data above is indicated a possibility that the 135.7-kev is an M1 mixed with some E2 transition. Now, looking at the L-subshell intensities for this transition, we have:

Multipolarity	Relative Intensities $L_I:L_{II}:L_{III}$
E1	2.3:1.0:0.8
E2	0.09:1.0:0.6
M1	11.0:1.0:0.4
M2	9.0:1.0:1.8
Observed	0.8: - : -

from which a pure E2 is eliminated. Combining the conclusions from these two sets of data, one can conclude that the 135.7-kev transition is an M1 (E2) transition.

An attempt was made to calculate the relative intensities of the transitions of Pa^{231}. From the electron intensities and known conversion coefficients the photon intensities were obtained. These

were compared with the photon intensities from the gamma spectrum of Hollander et al. The results are shown in Table XIV, where reasonable agreement was obtained except for the 84.1-kev transition, where if an E1 conversion coefficient was used the photon intensity was far too much compared to that obtained from the gamma spectrum. If a 30% M1 and 70% E2 is assumed, which is what the subshell ratios prefer, the calculated photon intensity is 5.8 compared to 7 ± 0.5 from the gamma spectrum. Since the accuracy of the electron intensities is about 20%, these are in agreement with each other. A plausible explanation for the disagreement of the calculated photon intensity with experiment of the 84.1-kev, if it is an E1, is that it is an "abnormal E1 transition," and in this case may also have a different conversion-electron coefficient, meaning to say it would be about five instead of 0.06, which is quite a big change. In view of all these disagreements the E1 assignment for the 84.1-kev should be considered tentative and be checked by other means.

TABLE XIV

COMPARISON OF TOTAL TRANSITION INTENSITIES

Transition Energy	Conv. Electron Intensity	Shell	Multipolarity	Conv. Coef.	Calc. Photon Intensity	Stephen's[64] Photon Intensity	Total Conv. Coef.	Total Electron Intensity	Total Trans. Intensity
17.2	6.1	M_{III}	E1	1.3	4.7		5	23	28
25.6	4.0	M_I	E1	0.28	14.3	12.5 ± 2	5	70	84
58.5	100.0	L_{II}	E2	65.0	1.5		184	276	278
68.5	0.8	L_{II}	E2	30.0	0.03		78	2	2
81.1	24.4	L_I	.7 M1 + .3 E2	6.2	3.9	3 ± 1	21	82	86
82.0	12.4	L_I	.5 M1 + .5 E2	4.6	2.7		26	70	73
84.1	35.9	L_I	E1	0.06	5.98	7 ± 0.5	1	419	1017
84.1	35.9	L_I	.3 M1 + .7 E2	6.2	5.8	7 ± 0.5	23.7	1375	143
99.3	5.2	L_I	M2	44.0	0.12	2 ± 0.5*	97	12	12
135.7	0.8	L_I	M1?	1.8	0.4	~ 0.2**	9	4	4
163.3	1.1	K	--	--	--	- 0.2	--	--	--
180	--	--	--	--	--	~ 0.05	--	--	--
218	--	--	--	--	--	0.05	--	--	--
310	--	--	--	--	--	0.003_5	--	--	--

* with K x-rays

** with 146.0-kev gamma rays

ACKNOWLEDGMENTS

I wish to express my sincere gratitude to Professor Isadore Perlman and Professor John Rasmussen, whose continuous encouragement and guidance have made this report possible.

I would like to thank Drs. J. M. Hollander, D. Strominger, F. S. Stephens, and S. G. Nilsson for many helpful and stimulating discussions.

The assistance of M. Brown, M. Firth, G. Killian, A. Larsh, M. Michel, F. Reynolds, and R. Watkins in the numerous instrumental problems associated with the instrument is deeply appreciated.

Some of the samples were kindly supplied by F. Asaro, T. Parsons, and R. Silva.

Finally, the Health Chemistry Group's consistent cooperation and concern on radiation hazard is sincerely acknowledged.

This work was performed under the auspices of the United States Atomic Energy Commission.

LIST OF TABLES

Table Number		Page Number
I.	Standards used in the calibration of the spectrometer....	35
II.	Conversion electron lines of Eu^{154}.....	46
III.	Gamma rays and coincidence abundances of Eu^{154}	49
IV.	Electron-electron coincidence of the 0.247- to 0.123-Mev transitions.....	53
V.	Conversion coefficients of the 0.123-Mev transition of Eu^{154}.....	57
VI.	Gamma-ray and conversion-electron absolute abundances of Eu^{154} and their multipolarity assignments.....	61
VII.	Beta groups of Eu^{154}.....	63
VIII.	Conversion electrons of Eu^{155}, their visual relative intensities, and multipolarity assignments.....	68
IX.	Conversion coefficients of the 86.4-kev transition of Eu^{155}.....	72
X.	Classification of Eu^{155} beta components.....	78
XI.	Calculated and experimental abundances of the beta components of Eu^{155} to the members of the rotational band of Gd^{155}.....	78
XII.	Beta components of Th^{231}.....	81
XIII.	Conversion electrons of Th^{231} and their relative intensities.....	86
XIV.	Comparison of total transition intensities of Th^{231}.....	97

LIST OF FIGURES

Figure Number		Page Number
1.	Electron-electron coincidence spectrometer.....	7
2.	Control and counting panel for the electron-electron coincidence spectrometer.....	8
3.	Longitudinal section of the electron spectrometer.....	10
4.	Spectrometer baffle system.....	13
5a.	Simplified wiring diagram of the main magnet coils, showing the number of turns.....	15
5b.	Simplified wiring diagram of the trimmer coils, showing the number of turns.....	18
6.	Magnet-current block diagram.....	20
7.	Fast-slow coincidence circuit block diagram.....	25
8a.	Cs^{137} conversion-electron picture at the ring-focusing position.....	29
8b.	Dimensions of aluminum ring-focusing baffle based on Fig. 8a picture.....	30
9.	Effect of the magnetic field of the opposite spectrometer on the Cs^{137} K-conversion-electron line when no trimmer coils are used.....	32
10.	Effect of the magnetic field of the opposite spectrometer on the L line of the 60-kev transition of Am^{241} with the proper trimmer coils.....	33
11.	Compensating effect of the trimmer coils on the opposite spectrometer with the beta spectrum of Cs^{137}.....	34
12.	Calibration curve of the spectrometer.....	36
13.	Calibration curve of the time-to-height converter (THC).....	38

Figure Number		Page Number
14.	THC coincidence spectrum for the 1064-kev $\longrightarrow$ 569-kev transition of Bi^{207}	40
15.	THC coincidence spectrum of a typical noncoincident transition pair	42
16a.	Portion of gamma-ray spectrum of Eu^{154}, showing resolution into five gamma rays and their relative intensities	48
16b.	Gamma-ray spectrum of Eu^{154} in coincidence with 0.12-Mev photons, showing resolution into five gamma rays and their relative intensities	50
17.	Gamma-ray spectrum of Eu^{154} in coincidence with 1.28-Mev photons	52
18.	Part of the beta-ray spectrum of Eu^{154} in coincidence with 0.12-Mev K-conversion electrons (normalized)	54
19.	Decay scheme of Eu^{154}	55
20.	Decay scheme of Eu^{155}	77
21.	Fermi plot of the beta spectrum of Th^{231}, showing resolution into their components	82
22.	Beta spectrum of Th^{231} as reconstructed from the Fermi-Kurie plot of Fig. 21	83
23.	Electron-counting efficiency of the G-M counter of the magnetic spectrometer, calculated from the Pm^{147} beta spectrum	85

REFERENCES

1. E. Persico and C. Geoffrion, Rev. Sci. Instr. 21, 945 (1950).
2. N. F. Verster, Progress in Nuclear Physics (Academic Press, New York, 1952), Vol. 2, p. 1.
3. K. Siegbahn, ed., Beta- and Gamma-Ray Spectroscopy (North Holland Publishing Company, Amsterdam, 1955).
4. K. Siegbahn, Arkiv Fysik 4, 223 (1952).
5. Pratt, Boley, and Nichols, Rev. Sci. Instr. 26, 92 (1951).
6. D. A. Thomas, "The Vanderbilt Beta-Ray Spectrometer and the Radioactive Decay of Tin-113," USAEC ORO-64, October 1952.
7. N. F. Moody, Electronic Eng. 24, 289 (1952).
8. Weber, Johnstone, and Cranberg, Rev. Sci. Instr. 27, 166 (1956).
9. Deutsch, Eliott, and Evans, Rev. Sci. Instr. 15, 178 (1944).
10. S. K. Haynes and J. W. Wedding, Rev. Sci. Instr. 22, 97 (1951).
11. T. O. Passell, "Internal Conversion of Gamma Radiation in the L Subshells" (Thesis), University of California Radiation Laboratory Unclassified Report UCRL-2528, 1954.
12. D. Strominger, "Experimental Study of Nuclear Isomers in the Millimicrosecond Lifetime Range" (Thesis), University of California Radiation Laboratory Unclassified Report UCRL-3374, 1956.
13. C. W. Johnstone, Nucleonics 11, 36 (1953).
14. A. Ghiorso and A. E. Larsh, in Chemistry Division Quarterly Report, UCRL-2647, July 1954.
15. B. D. Pate and L. Yaffe, Canadian J. Chem. 33, 15 (1955).
16. M. I. Kalkstein and J. M. Hollander, "A Survey of Counting Efficiencies for a 1.5-Inch-High Sodium Iodide (Thallium Activated) Crystal," University of California Radiation Laboratory Report UCRL-2764, 1954.
17. Pohm, Lewis, Talboy, and Jensen, Phys. Rev. 95, 1523 (1954).

18. P. B. Day, Phys. Rev. 97, 689 (1955).

19. Wapstra, Maeder, Nijgh, and Ornstein, Physica 20, 169 (1954).

20. D. E. Alburger and A. W. Sunyar, Phys. Rev. 99, 695 (1955).

21. A. I. Yavin and F. H. Schmidt, Phys. Rev. 100, 171 (1955).

22. Document UIP6 (1955) of International Union of Pure and Applied Physics, in Physics Today 9, No. 11, 23 (1956).

23. M. Brown, "Millimicrosecond Coincidence Instrumentation and its Limitations," University of California Radiation Laboratory Unclassified Report UCRL-3539, 1956.

24. T. R. Gerholm, Arkiv Fysik 10, 523 (1956).

25. T. C. Engelder, Phys. Rev. 90, 259 (1953).

26. H. Scheichenberger, Anz. Akad. Wiss. Wien. Math. -naturw. Klasse 75, 108 (1938).

27. Karraker, Hayden, and Inghram, Phys. Rev. 87, 901 (1952).

28. E. L. Church and M. Goldhaber, Phys. Rev. 95, 626A (1954).

29. Cork, Keller, Rutledge, and Stoddard, Phys. Rev. 77, 848 (1950).

30. F. Boehm and E. N. Hatch, Nuclear Data Card No. 57-1-95 (1957). (National Research Council, Washington, D. C.).

31. Cork, Shreffer, and Fowler, Phys. Rev. 74, 240 (1948).

32. Slattery, Lu, and Wiedenbeck, Phys. Rev. 96, 465 (1954).

33. M. R. Lee and R. Katz, Phys. Rev. 93, 155 (1954).

34. B. Andersson, Proc. Phys. Soc. 69A, 415 (1956), (London).

35. A. W. Sunyar, Phys. Rev. 98, 653 (1955).

36. Huus, Bjerregaard, and Elbek, Kgl. Danske Vidensk. Selskab Mat. fys. Medd. 30, No. 17 (1956).

37. Kedzie, Abraham, and Jeffries, Bull. Am. Phys. Soc. 1, 390 (1956).

38. F. S. Stephens, Jr., "Decay Schemes and Nuclear Spectroscopic States in the Heavy-Element Region " (Thesis), University of California Radiation Laboratory Unclassified Report UCRL-2970, 1955.

39. W. G. Smith and J. M. Hollander, Phys. Rev. 101, 746 (1956).

40. G. D. O'Kelley, "The Spectrometric Determination of Some Beta Particle and Conversion Electron Energies " (Thesis), University of California Radiation Laboratory Unclassified Report UCRL-1243, 1951.

41. Cork, Brice, Helmer, and Sarason, Bull. Am. Phys. Soc. 2, 16 (1957).

42. K. Toth (unpublished data).

43. P. R. Gray, Phys. Rev. 101, 1306 (1956).

44. L. A. Sliv (privately circulated tables).

45. M. E. Rose (privately circulated tables).

46. A. Bohr and B. R. Mottelson, Kgl. Danske Videnskab. Selskab. Mat fys. Medd. 27, No. 16 (1953).

47. Rasmussen, Slätis, Passell, Stephens, Strominger, and Ström, Phys. Rev. 99, 47 (1955).

48. H. W. Wilson and G. M. Lewis, Proc. Phys. Soc. (London) A65, 656 (1952).

49. Dubey, Mandeville, and Rothman, Phys. Rev. 103, 1430 (1956).

50. E. L. Church, Preprint, June 1956, as quoted in B. Mottelson and S. Nilsson's article to be published in Kgl. Danske Videnskab. Selskab. Mat. fys. Medd.

51. Rutledge, Cork, and Burson, Phys. Rev. 86, 775 (1952).

52. J. H. Bjerregaard and U. Meyer-Berkhout, Z. Naturforsch. 11a, 273 (1956).

53. N. P. Heydenburg and G. M. Temmer, Phys. Rev. 104, 981 (1956).

54. Alder, Bohr, Huus, Mottelson, and Winther, Revs. Modern Phys. 28, 432 (1956).

55. F. A. Jenkins and D. R. Speck, Phys. Rev. 100, 973A (1955).

56. D. R. Speck, Phys. Rev. 100, 1725 (1956).

57. S. G. Nilsson, Kgl. Danske Videnskab. Selskab, Mat. fys. Medd. 29, No. 16 (1955).

58. Alaga, Alder, Bohr, and Mottelson, Kgl. Danske Videnskab. Selskab, Mat. fys. Medd. 29, No. 9 (1955).

59. G. Alaga, Phys. Rev. 100, 432 (1955).

60. E. U. Condon and G. H. Shortley, Theory of Atomic Spectra (Cambridge University Press, London, 1935).

61. A. H. Jaffey and E. K. Hyde, NSA 6H21 (1949).

62. Freedman, Jaffe, Wagner, and May, Phys. Rev. 89, 302 (1953).

63. J. P. Mize and J. W. Storner, Bull. Am. Phys. Soc. No. 4, 171 E61 (1956).

64. Hollander, Asaro, and Stephens (unpublished data).

65. D. Strominger and J. O. Rasmussen, Phys. Rev. 100, 844 (1955).

66. J. O. Newton (unpublished data).

67. Asaro and Stephens (private communication).